

# Chemical abundances and kinematics of a sample of metal-rich barium stars $\star, \star\star$

C.B. Pereira<sup>1</sup>, J.V. Sales Silva<sup>1</sup>, C. Chavero<sup>1</sup>, F. Roig<sup>1</sup> & E. Jilinski<sup>1,2</sup>

<sup>1</sup> Observatório Nacional, Rua José Cristino, 77. CEP 20921-400. São Cristóvão. Rio de Janeiro-RJ. Brazil.

<sup>2</sup> Instituto de Física, Universidade do Estado do Rio de Janeiro, Rua São Francisco Xavier 524, Maracanã, 200550-900 Rio de Janeiro-RJ, Brazil  
e-mail: claudio, joao, victor, carolina, froig, jilinski@on.br

Received ; accepted

## ABSTRACT

**Aims.** We determined the atmospheric parameters and abundance pattern for a sample of metal-rich barium stars.

**Methods.** We used high-resolution optical spectroscopy. Atmospheric parameters and abundances were determined using the local thermodynamic equilibrium atmosphere models of Kurucz and the spectral analysis code MOOG.

**Results.** We show that the stars have enhancement factors, [s/Fe], from 0.25 to 1.16. Their abundance pattern of the Na, Al,  $\alpha$ -elements, and iron group elements as well as their kinematical properties are similar to the characteristics of the other metal-rich and super metal-rich stars already analyzed. We conclude that metal-rich barium stars do not belong to the bulge population. We also show that metal-rich barium stars are useful targets for probing the s-process enrichment in high-metallicity environments.

**Key words.** stars: abundances — stars: chemically peculiar — stars: barium stars

## 1. Introduction

Barium stars are chemically peculiar giant stars displaying both anomalously high heavy-element ( $Z > 30$ ) abundances and an overabundance of carbon compared to the Sun, with  $[C/Fe]$  varying from +0.4 to +1.2 (Antipova et al., 2004; Allen & Barbuy, 2006; Drake & Pereira, 2008; Pereira & Drake, 2009). In the mass-transfer hypothesis, the observed chemical peculiarities of these stars are a consequence of mass transfer through stellar winds or through Roche-lobe overflow in a binary system from an AGB star (now the white dwarf) to a less evolved companion, a barium giant or a subgiant CH star. Therefore, the study of their chemical peculiarities is important for understanding the physics of accretion phenomena in chemically peculiar binary systems.

Barium giants are the largest known sample among the chemically peculiar stars where the effects of the s-process nucleosynthesis can be widely investigated and measured. Busso et al. (2001) use the  $[hs/ls]$ <sup>1</sup> index as a function of metallicity as a criterion to probe whether the current models of s-process nucleosynthesis in AGB stars account for the observed abundance distributions.

Barium stars are found in the disk and in the halo of the Galaxy according to Gomez et al. (1997) and Mennessier et al. (1997). These two studies show that barium stars are an inho-

mogeneous group that can also be divided into groups according to their luminosities, kinematical and spatial parameters ( $U_0$ ,  $V_0$ ,  $W_0$  velocities and dispersion velocities and scale heights). If the barium star phenomenon is seen both in the disk and in the halo, they are very useful objects to probe the s-process nucleosynthesis at different metallicities, in different population. Barium stars have already been analyzed in the halo, such as HD 206983 (Junqueira & Pereira, 2001; Drake & Pereira, 2008), HD 10613 (Pereira & Drake, 2009), and HD 123396 (Allen & Barbuy, 2006), and their connection with the metal-poor halo yellow symbiotic stars have already been investigated (Jorissen et al., 2005; Pereira & Drake, 2009). Therefore, the quantitatively confirmation of the overabundances of the s-process elements in a sample of barium stars would help to better constrain the number of known barium stars, which it would be useful to compare with their theoretical birthrate (Han et al., 1995). Motivated by the questions mentioned above, we started a high-resolution spectroscopic survey of the barium stars from the samples of MacConnell et al. (1972) and Bidelman (1981) as well as some stars from Gomez et al. (1997). As a first result of 230 surveyed stars, we have already discovered a new CH subgiant, BD-03°3668 (Pereira & Drake, 2011).

In this paper we report another result from our survey, that is, the discovery of a small sample of 12 metal-rich ( $[Fe/H] \geq +0.1$ ) barium stars. According to their metallicities, metal-rich stars can be divided into two sub-samples (Grenon, 1972). Stars with metallicities  $0.08 < [Fe/H] < +0.2$  are the metal-rich ones and those with metallicities  $+0.2 < [Fe/H] < +0.5$  are the super metal-rich. According to this scheme, we found 7 metal-rich and 5 super metal-rich barium stars. The “very metal-rich” stars were first identified by Arp (1965) investigating the nucleus of the galaxy NGC 6522. Arp (1965) also derived their age to be between  $10^9$  to  $10^{10}$  Gyr. Spinrad & Taylor (1969) surveyed a large

Send offprint requests to: C.B. Pereira

\* Based on observations made with the 1.52m and 2.2m telescope at the European Southern Observatory (La Silla, Chile).

\*\* Tables 2 and 4 are only available in electronic form at the CDS via anonymous ftp to cdsarc.u-strasbg.fr (130.79.128.5) or via <http://cdsweb.u-strasbg.fr/cgi-bin/qcat?J/A+A/>.

<sup>1</sup>  $[hs/ls] = \log(hs/ls)_\star - \log(hs/ls)_\odot$  where  $[hs]$  and  $[ls]$  are the mean abundances of the s-elements at the Ba and Zr peaks, respectively.

group of K giants with metal abundances greater than that of the Hyades and with abundance variations among their sample. These authors also found the giants ages to be older than the disk star, Grenon (1999) also showed that metal-rich stars have an age mixture ranging from 0.7 Gyr for the Hyades generation to an intermediate generation of 3-4 Gyr and to an oldest generation, 10 Gyr. In the investigation of the photometric and kinematic properties of a large sample of G and K giants, Eggen (1993) found that 10% of the stars in the solar neighborhood have metallicities higher than +0.15 dex. Eggen (1993) also identified a sample of barium stars among the evolved stars in the old disk population that could be metal-rich as well. However, none of the stars presented in Table 11 of his paper can be classified as metal-rich or super metal rich (HD 46407,  $[Fe/H] = -0.14$ , Antipova et al. (2003); HD 116713 and HD 202109 with respectively  $[Fe/H] = -0.12$  and -0.04, Smiljanic et al. (2007); HD 83548,  $[Fe/H] = +0.03$ , Pereira et al. (2011); and NGC 2420 - D,  $[Fe/H] = -0.55$ , Smith & Suntzeff (1987)). Metal-rich stars have a mean distance from the Galactic plane of 0.2 kpc and and their Galactic orbits appear to be located inside the solar Galactic orbit (Grenon, 1999). Metal-rich stars in the solar neighborhood either could be diffused into the disk from the bulge population (Barbuy & Grenon, 1990) or they may be the representatives of the last stages of the chemical evolution of the disk (Matteucci, 2003).

We here analyze the high-resolution spectra of a sample of metal-rich barium stars to obtain  $[X/Fe]$  versus  $[Fe/H]$  trends and also to investigate the heavy-element abundance pattern in metal-rich environments. As we shall see, all our stars have spectral types G and K, and are accordingly free from the strong molecular opacity from ZrO, CN and C<sub>2</sub> absorption features, which complicates a quantitative analysis and the measurement of some atomic lines. These molecules are usually observed in MS, S, and disk carbon stars at near solar metallicity where enhancements from s-process nucleosynthesis have already been reported (Busso et al., 2001).

## 2. Observations

The high-resolution spectra of our stars were obtained with the FEROS (Fiberfed Extended Range Optical Spectrograph) Echelle spectrograph (Kaufer et al., 1999) at the 1.52 m and 2.2 m ESO telescopes at La Silla (Chile) in several runs between 2000 and 2010. The FEROS spectral resolving power is  $R = 48\,000$ , corresponding to 2.2 pixels of  $15\,\mu\text{m}$ , and the wavelength coverage goes from  $3\,800\,\text{\AA}$  to  $9\,200\,\text{\AA}$ . The nominal  $S/N$  ratio was evaluated by measuring the rms flux fluctuation in selected continuum windows, and the typical values were  $S/N = 100 - 200$ . The spectra were reduced with the MIDAS pipeline reduction package consisting of the following standard steps: CCD bias correction, flat-fielding, spectrum extraction, wavelength calibration, correction of barycentric velocity, and spectrum rectification. Table 1 shows the log of observations and some previous information (V-magnitude, spectral types and the literature sources from where the stars were selected) of the studied stars.

## 3. Analysis and results

### 3.1. Line selection, measurements, and oscillator strengths

Several atomic absorption lines used in this study are the same as were used in previous studies dedicated to the analysis of photospheric abundances of the barium stars (Pereira, 2005;

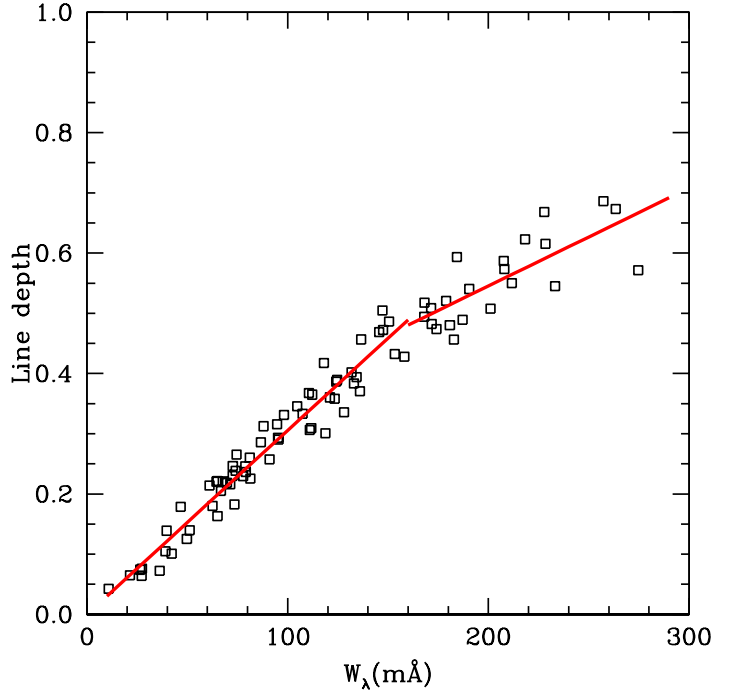


**Fig. 1.** Line depth vs. equivalent width of Fe I lines of CD-25 6606. This plot shows that there is a change in the slope around  $160\,\text{m}\text{\AA}$  which was used to set this limit for the equivalent widths in our abundance analysis.

Pereira & Drake, 2009, 2011). The chosen lines are sufficiently unblended to yield reliable abundances. Table 2 shows the Fe I and Fe II lines employed in the analysis and also the lower excitation potential,  $\chi(\text{eV})$ , of the transitions, the  $\log g f$  values, and the measured equivalent widths. The latter were obtained by fitting Gaussian profiles to the observed ones. The  $\log g f$  values for the Fe I and Fe II lines were taken from Lambert et al. (1996) and Castro et al. (1997).

Absorption lines whose equivalent widths are not stronger than  $150\,\text{m}\text{\AA}$  should lie in the linear part of the curve of growth (Hill et al., 1995). We can evaluate if this limit is also valid for our measurements of equivalent widths by analyzing a plot of line depth vs. equivalent width. In this kind of plot we aim to examine whether (and where) there would be a significant change in the behavior of the absorption lines when the weaker and stronger lines are studied together. Figure 1 shows these measurements of several Fe I lines in the spectrum of CD-25 6606. We fitted the data using two linear functions, one between  $0.0\,\text{m}\text{\AA}$  and  $W_{\text{turn}}$ , and another between  $W_{\text{turn}}$  and  $300\,\text{m}\text{\AA}$ . By varying the value of  $W_{\text{turn}}$  between  $100$  and  $200\,\text{m}\text{\AA}$  we verified that the best fits for the two linear functions simultaneously hold for  $W_{\text{turn}} \sim 160 - 170\,\text{m}\text{\AA}$ . At this point, the slope shows a reduction of about 50% (from  $\sim 0.0031$  to  $\sim 0.0017$ ). Figure 1 also shows that up to  $\sim 160\,\text{m}\text{\AA}$  the  $\chi^2$  of fit is lower (0.0008) than the  $\chi^2$  between  $160$  and  $300\,\text{m}\text{\AA}$ , which is 0.002. The change of slope and the large dispersion upward of  $160\,\text{m}\text{\AA}$  are caused by saturation effects that become important for the stronger lines so that the Gaussian profiles would not be the best representation for the line profiles. Therefore, lines with equivalent widths stronger than  $160\,\text{m}\text{\AA}$  were not used in our abundance analysis for the stars analyzed in this work. For the same reason we did not use any of the barium lines in our sample stars.

**Table 1.** Log of the observations and basic information of the stars.

Star	Date	Exposure time (sec)	V (mag)	SpT <sup>a</sup>	Source
CD-25 6606	22/02/2008	1 200	9.3	—	II <sup>b</sup>
HD 46040	14/10/2008	420	8.0	K0p	I <sup>c</sup>
HD 49841	27/01/2001	3 600	9.0	G5	I
HD 82765	17/02/2008	600	8.5	G8 III	II
HD 84734	17/02/2008	600	9.0	—	II
HD 85205	25/03/2000	720	8.4	G6 II	II
HD 100012	13/02/2008	420	6.6	K0/K1 III	II
HD 101079	03/04/2007	600	8.2	K2	B81 <sup>d</sup>
HD 130386	28/07/2009	420	7.8	K2	II
HD 139660	03/04/2007	900	8.4	K0	G97 <sup>e</sup>
HD 198590	18/08/2008	360	7.0	G8 II	II
HD 212209	18/08/2008	600	8.9	—	II

a: Gomez et al. (1997)

b: Table II of MacConnell et al. (1972)

c: Table I of MacConnell et al. (1972)

d: Bidelman (1981)

e: Gomez et al. (1997)

### 3.2. Determination of the atmospheric parameters

The determination of stellar atmospheric parameters effective temperature ( $T_{\text{eff}}$ ), surface gravity ( $\log g$ ), microturbulence ( $\xi$ ), and [Fe/H] (throughout, we use the notation  $[X/H]=\log(N(X)/N(H))_* - \log(N(X)/N(H)_{\odot})$ ) are prerequisites for the determination of photospheric abundances. The atmospheric parameters were determined by assuming local thermodynamic equilibrium (hereafter LTE) model atmospheres of Kurucz (1993) using the spectral analysis code MOOG (Sneden, 1973).

The solution of the excitation equilibrium used to derive the temperature ( $T_{\text{eff}}$ ) was defined by the zero slope of the trend between the iron abundances derived from FeI lines and the excitation potential of the measured lines. The microturbulent velocity ( $\xi$ ) was determined by constraining the abundance determined from individual Fe I lines to show no dependence on  $W_{\lambda}/\lambda$ . The solution thus found is unique, depending only on the set of Fe I,II lines and the atmospheric model employed, and yields as a by-product the metallicity of the star [Fe/H]. The final adopted atmospheric parameters are given in Table 3. The value of  $\log g$  seen in Table 3 was determined by means of the ionization balance using the assumption of LTE. We found typical uncertainties of  $\sigma(T_{\text{eff}}) = 150$  K,  $\sigma(\log g) = 0.2$  dex, and  $\sigma(\xi) = 0.2$  km s<sup>-1</sup>.

Previous determinations of atmospheric parameters of two stars of our sample, HD 100012 and HD 130386, were made by Luck & Bond (1991) and Antipova et al. (2004), respectively. Luck & Bond (1991) found for HD 100012,  $T_{\text{eff}} = 5000$  K,  $\log g = 2.3$  dex,  $V_t = 2.2$  km s<sup>-1</sup> and [Fe/H] = +0.33, while for HD 130386, Antipova et al. (2004) found  $T_{\text{eff}} = 4720$  K,  $\log g = 2.4$  dex,  $V_t = 1.4$  km s<sup>-1</sup> and [Fe/H] = 0.01 dex.

### 3.3. Abundance analysis

The abundances of chemical elements were determined with the LTE model atmosphere techniques. In brief, equivalent widths are calculated by integration through a model atmosphere and are compared with the observed equivalent widths. The calculations are repeated, changing the abundance of the element in question, until a match is achieved. The current version of the line-synthesis code moog (Sneden, 1973) was used to carry out the calculations. Table 4 shows the atomic lines used to derive

the abundances of the elements. Atomic parameters for several transitions of Ti, Cr, and Ni were retrieved from the library of the National Institute of Science and Technology Atomic Spectra Database (Martin et al., 2002). Tables 5 and 6 provide the derived abundances in the notation [X/Fe]. The last two columns of Table 6 give the mean abundance of the s-process elements and their standard deviations, i.e., the scatter around the mean.

### 3.4. Abundance uncertainties

The uncertainties of the derived abundances for the program stars are dominated by two main sources: the errors in the stellar parameters and errors in the equivalent width measurements.

The abundance uncertainties owing to the errors in the stellar atmospheric parameters  $T_{\text{eff}}$ ,  $\log g$ , and  $\xi$  were estimated by changing these parameters by their standard errors and then computing the changes incurred in the element abundances. This technique was applied in the abundances determined from equivalent line widths. The results of these calculations for CD-25°6606 are displayed in columns 2 to 5 of Table 7. The abundance variations for the other stars show similar values.

The abundance uncertainties owing to the errors in the equivalent widths measurements were computed from an expression provided by Cayrel (1988). The errors in the equivalent widths are set, essentially, by the signal-to-noise ratio and the resolution of the spectra. In our case, having  $R \approx 50\,000$  and typical S/N of 150, the expected uncertainties in the equivalent widths are about 2–3 mÅ. For all measured equivalent widths, these uncertainties lead to the errors in the abundances less than those from the sum of the uncertainties owing to the stellar parameters.

Under the assumption that the errors are independent, they can be combined quadratically so that the total uncertainty is

$$\sigma = \sqrt{\sum_{i=1}^N \sigma_i^2}$$

These final uncertainties are given in the sixth column of Table 7. The last column gives the observed abundance dispersion among the lines for those elements with more than three available lines. Table 7 also shows that neutral elements are fairly sensitive to the temperature variations, while single ionized elements are sensi-

**Table 3.** Atmospheric parameters, radial velocities, and galactic latitude.

	$T_{\text{eff}}$ (K)	$\log g$	[FeI/H]	[FeII/H]	$\xi$ ( $\text{km s}^{-1}$ )	$V_r$ ( $\text{km s}^{-1}$ )	latitude gal. ( $b^\circ$ )
CD-25 6606	5300	2.7	+0.12 ± 0.14 (55)	+0.10 ± 0.09 (10)	1.5	+0.99 ± 0.91	+11.04
HD 46040	4800	2.4	+0.11 ± 0.13 (27)	+0.11 ± 0.14 (9)	1.4	+23.72 ± 0.33	-29.59
HD 49841	5200	3.2	+0.21 ± 0.13 (55)	+0.20 ± 0.19 (12)	1.3	+8.17 ± 0.50	+02.40
HD 82765	5100	2.6	+0.19 ± 0.10 (43)	+0.20 ± 0.11 (11)	1.4	+10.53 ± 0.49	-10.65
HD 84734	5200	2.9	+0.20 ± 0.12 (40)	+0.21 ± 0.11 (11)	1.5	-27.38 ± 2.81	-11.68
HD 85205	5300	2.8	+0.23 ± 0.16 (41)	+0.24 ± 0.09 (12)	1.9	+25.31 ± 0.58	+13.70
HD 100012	5000	2.7	+0.18 ± 0.12 (45)	+0.19 ± 0.10 (11)	1.5	+8.95 ± 0.65	+33.59
HD 101079	5000	2.7	+0.10 ± 0.12 (52)	+0.09 ± 0.08 (11)	1.3	-2.77 ± 0.55	+56.64
HD 130386	4900	2.7	+0.16 ± 0.13 (39)	+0.14 ± 0.11 (10)	1.3	+16.46 ± 0.45	+46.88
HD 139660	5000	2.8	+0.26 ± 0.14 (44)	+0.26 ± 0.11 (12)	1.4	-13.22 ± 0.54	+35.11
HD 198590	5100	2.6	+0.18 ± 0.14 (48)	+0.17 ± 0.13 (11)	1.5	-9.62 ± 0.42	-39.51
HD 212209	4700	2.4	+0.30 ± 0.13 (38)	+0.30 ± 0.13 (10)	1.2	-27.23 ± 0.52	-48.29

**Table 5.** Abundance ratios [X/Fe] for the elements from Na to Ni.

star	[Na/Fe]	[Mg/Fe]	[Al/Fe]	[Si/Fe]	[Ca/Fe]	[Ti/Fe]	[Cr/Fe]	[Ni/Fe]
CD-25 6606	+0.19	+0.05	-0.02	+0.11	+0.08	-0.04	+0.03	0.00
HD 46040	+0.16	+0.04	+0.02	-0.09	+0.11	+0.03	+0.06	-0.04
HD 49841	+0.04	-0.08	-0.11	-0.03	+0.07	-0.01	0.00	+0.02
HD 82765	+0.15	+0.18	+0.06	+0.15	+0.14	0.00	+0.06	+0.08
HD 84734	+0.12	+0.19	-0.08	+0.21	+0.06	+0.01	+0.05	+0.03
HD 85205	+0.23	+0.11	+0.11	+0.09	+0.08	-0.05	-0.01	+0.08
HD 100012	+0.29	+0.19	0.00	+0.15	+0.05	+0.04	0.00	+0.06
HD 101079	+0.20	+0.14	+0.23	+0.19	+0.10	-0.06	+0.02	+0.03
HD 130386	+0.36	+0.19	+0.21	+0.19	+0.15	+0.09	+0.03	+0.09
HD 139660	+0.23	+0.06	+0.07	+0.19	+0.07	-0.05	+0.03	+0.05
HD 198590	+0.21	+0.20	+0.16	+0.22	+0.10	-0.09	-0.02	+0.03
HD 212209	+0.15	+0.12	+0.18	+0.20	+0.06	-0.03	0.00	+0.07

**Table 6.** Abundance ratios [X/Fe] for the heavy elements.

star	[Y/Fe]	[Zr/Fe]	[La/Fe]	[Ce/Fe]	[Nd/Fe]	[s/Fe]	$\sigma([s/\text{Fe}])$
CD-25 6606	+0.62	+0.48	+0.73	+0.52	+0.85	+0.64	0.15
HD 46040	+0.93	+1.04	+1.83	+1.07	+0.94	+1.16	0.38
HD 49841	+0.85	+0.65	+0.81	+0.56	+0.92	+0.76	0.15
HD 82765	+0.52	+0.37	+0.35	+0.12	+0.20	+0.31	0.14
HD 84734	+0.64	+0.60	+0.74	+0.56	+0.80	+0.67	0.10
HD 85205	+0.65	+0.65	+0.58	+0.44	+0.80	+0.62	0.14
HD 100012	-0.03	+0.13	+0.29	+0.25	+0.45	+0.22	0.18
HD 101079	+0.63	+0.44	+0.43	+0.28	+0.51	+0.46	0.13
HD 130386	+0.65	+0.59	+0.47	+0.47	+0.29	+0.49	0.14
HD 139660	+0.77	+0.51	+0.56	+0.35	+0.50	+0.54	0.15
HD 198590	+0.69	+0.51	+0.38	+0.33	+0.33	+0.45	0.15
HD 212209	+0.53	+0.24	+0.24	+0.06	+0.18	+0.25	0.17

tive to the  $\log g$  variations. The uncertainties on microturbulence also contribute to the compounded errors.

#### 4. Discussion

##### 4.1. The position of the stars in the $\log g$ - $\log T_{\text{eff}}$ diagram.

Figure 2 shows the position of the studied stars in the  $\log T_{\text{eff}}$  -  $\log g$  diagram, where model tracks were computed by Schaefer et al. (1993) for the stars of 2.0, 2.5, and 3.0 solar masses with metallicity of  $Z = 0.04$ . Putting the studied stars in this diagram, we estimated the masses as given in Table 8. Table 8 also provides the distance that resulted from the assumed mass from the  $\log T_{\text{eff}}$  -  $\log g$  diagram and from the temperature and surface gravity given in Table 3. In these calculations we assumed the bolometric corrections of Alonso et al. (1999) and  $M_{\text{bol}\odot} = +4.74$  (Bessell et al., 1998). The last column of Table 8 provides the distance of the stars whose parallax were measured

by Hipparcos. The distances were derived based on the ionization equilibrium and the derived masses from the positions in the  $\log g$  -  $\log T_{\text{eff}}$  diagram, and astrometric values agree well within the uncertainties with the possible exception of HD 13966.

The stars CD-25 6606, HD 49841, HD 84734, and HD 85205, with  $\log T_{\text{eff}} = 3.72$  and  $\log g = 2.7, 3.2, 2.9$ , and 2.8 respectively, occupy a region that is at the end of subgiant phase or near the base of red giant branch in the  $\log g$  -  $\log T_{\text{eff}}$  diagram. This is important because in all high-resolution spectroscopy studies dedicated to the analyses of the spectra of barium dwarfs and CH subgiant stars, no stars of near solar metallicity or even higher than the solar metallicity in this evolutionary phase were found (Smith et al., 1993; Pereira, 2005; Allen & Barbuy, 2006). Therefore, these four stars might be the first identified metal-rich CH subgiants. Barium dwarfs ( $\log g \geq 4.0$ ) with metallicities close to the solar one are as yet undiscovered (Pereira & Drake, 2011).

**Table 7.** Abundance uncertainties for CD-25 6606. The second column gives the variation of the abundance caused by the variation in  $T_{\text{eff}}$ . The other columns refer to the variations caused by  $\log g$ ,  $\xi$ , and  $W_{\lambda}$ , respectively. The sixth column gives the compounded r.m.s. uncertainty of the second to fifth columns. The last column gives the observed abundance dispersion for those elements whose abundances were derived using more than three lines.

Species	$\Delta T_{\text{eff}}$ +150 K	$\Delta \log g$ +0.3	$\Delta \xi$ +0.3	$\Delta W_{\lambda}$ +3 mÅ	$(\sum \sigma^2)^{1/2}$	$\sigma_{\text{obs}}$
Fe I	+0.12	0.00	-0.13	+0.07	0.19	0.14
Fe II	-0.09	+0.11	-0.14	+0.07	0.21	0.09
Na I	+0.10	-0.01	-0.06	+0.06	0.13	0.15
Mg I	+0.05	-0.03	-0.06	+0.04	0.09	0.18
Al I	+0.07	-0.02	-0.05	+0.05	0.10	0.19
Si I	+0.01	+0.02	-0.05	+0.06	0.08	0.06
Ca I	+0.13	-0.01	-0.14	+0.07	0.20	0.10
Ti I	+0.28	+0.01	-0.07	+0.07	0.29	0.09
Cr I	+0.15	+0.02	-0.09	+0.08	0.19	0.18
Ni I	+0.11	+0.03	-0.10	+0.07	0.17	0.12
Y II	+0.01	+0.12	-0.16	+0.08	0.22	0.06
Zr I	+0.21	+0.02	-0.01	+0.08	0.23	0.04
La II	+0.02	+0.13	-0.06	+0.07	0.16	0.19
Ce II	+0.02	+0.13	-0.09	+0.08	0.18	0.11
Nd II	+0.04	+0.15	-0.15	+0.10	0.24	0.14

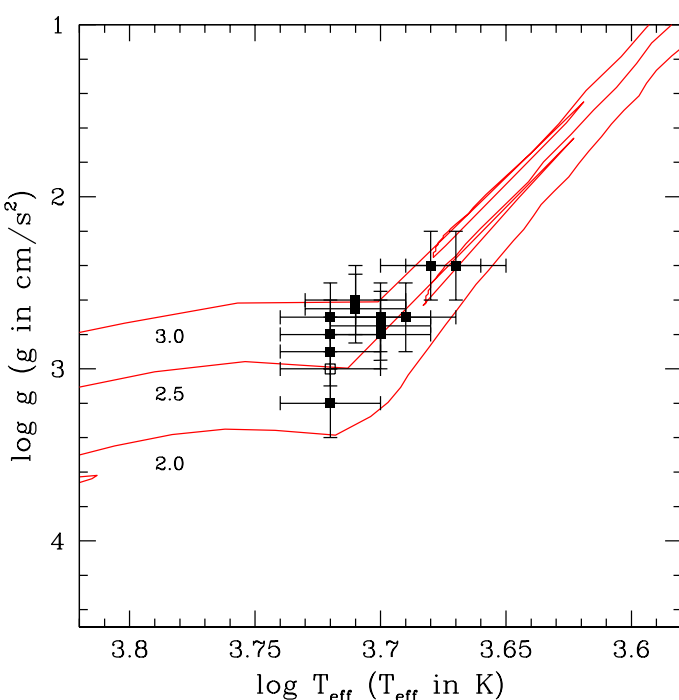


**Fig. 2.** Position of the stars (filled squares) in the  $\log g$  –  $\log T_{\text{eff}}$  diagram. Evolutionary tracks are from Schaerer et al. (1993). The numbers correspond to stellar masses in units of solar mass. Red lines represent evolutionary tracks for a star with  $Z = 0.04$ . The stars CD-25 6606, HD 49841, HD 84734, and HD 85205 are subgiant stars about to begin their ascent of the red giant branch, like S 190, a D'-type symbiotic star (open square) that is also barium enriched (Smith et al., 2001).

#### 4.2. Kinematics

As we mentioned in the introduction, some metal-rich stars could be old objects. Figure 3 shows the position of stars analyzed in this work in the HR-diagram with the isochrones of

**Table 8.** Masses and distances of the stars.

star	$M/M_{\odot}$	r (pc)	r (pc)(Hipparcos)
CD-25 6606	3.0	820±200	—
HD 46040	2.5	440±100	320±70
HD 49841	2.0	310±70	—
HD 82765	2.5	520±120	420±140
HD 84734	2.5	490±115	—
HD 85205	2.5	440±100	—
HD 100012	2.5	190±45	180±25
HD 101079	2.5	390±90	—
HD 130386	2.5	300±70	290±110
HD 139660	2.5	380±90	190±44
HD 198590	2.5	260±60	410±140
HD 212209	2.5	630±150	390±180

Girardi et al. (2000). The metal-rich barium stars with ages between 8.5 and 9.0 Gyr are similar to the metal-rich stars analyzed by Pakhomov et al. (2009), which have a mean age of  $\approx 8.7$  Gyr. Our results confirm the results of Mennessier et al. (1997) that some barium stars in this range of gravity (and also in absolute magnitudes) have ages between 8.5 and 9.5 Gyr.

We also investigated the kinematical properties of our sample stars. Table 9 shows our results. The radial velocities were determined by measuring the Doppler shift of the spectral lines and are given in Table 3. Distances and proper motions were taken from the Hipparcos catalog (Perryman & ESA, 1997). Space velocities ( $U_{\odot}$ ,  $V_{\odot}$ ,  $W_{\odot}$ ) relative to the local standard of rest were computed based on the method of Johnson & Soderblom (1987) and were calculated assuming the solar motion of  $(U, V, W) = (11.1, 12.2, 7.3) \text{ km s}^{-1}$ , as derived by Schönrich et al. (2010). The Galactic orbital parameters  $R_{\min}$  and  $R_{\max}$  (minimum and maximum distances from the Galactic center),  $Z_{\max}$  (maximum distance from Galactic plane) and  $e$  (orbital eccentricity) were obtained using the Galactic potential integrator developed by C. Flynn (<http://www.astro.utu.fi/galorb.html>). For this we adopted a solar Galactocentric distance of 8.5 kpc and circular velocity of  $220 \text{ km s}^{-1}$ . Because barium stars are binary stars, their observed radial velocities are affected by periodical variations. If we have

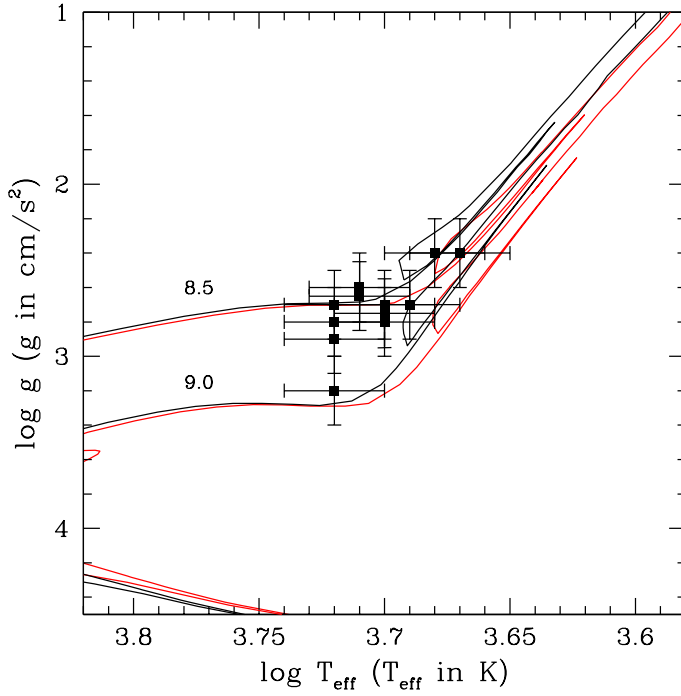


**Fig. 3.** Positions of the metal-rich barium stars compared with isochrones of Girardi et al. (2000). Red lines represent metallicities of  $Z=0.03$  and black lines represent metallicities of  $Z=0.02$ . The numbers correspond to the age in units of Gyr.

only one determination of radial velocity, it is interesting to evaluate the uncertainties introduced by an unknown orbital motion. For this purpose we analyzed observed orbital velocity amplitude of barium binary stars with determined orbital elements (Jorissen & Mayor, 1988; Udry et al., 1998b,a). Figure 4 shows the dependence between observed orbital velocity amplitudes and the periods of analyzed stars. The mean value of the amplitude for the whole sample was found to be  $6 \text{ km s}^{-1}$ . This value was considered as the uncertainty in the determined radial velocities of our stars.

Inspecting Table 9 we may conclude that our sample stars come from several places of the Galaxy, with mean space velocities of  $U_{LSR}=6\pm23$ ,  $V_{LSR}=-6\pm16$  and  $W_{LSR}=5\pm13 \text{ km s}^{-1}$ . Their minimum and maximum distances to the Galactic center are  $7.3\pm0.6 \text{ kpc}$  and  $8.5\pm0.8 \text{ kpc}$ , respectively. Most of the stars have  $V_{LSR}$  negative results, which can be taken as indication that they lag in the Galactic rotation compared to the solar motion. Two stars, HD 198590 and HD 212209, have  $V_{LSR}$  opposite velocities compared to the rest of the stars. These properties can be taken as evidence that these metal-rich barium stars as well as other metal-rich and super metal-rich stars form an inhomogeneous group. Metal-rich stars with space velocities and/or  $R_{min}$  and  $R_{max}$  that differ from each other of the same studied sample would have a different star-formation history and evolution (Pakhomov et al., 2009). It is also interesting to notice that HD 212209 has the highest eccentricity among the other stars. Most of the stars have  $R_{max}$  less than  $8.5 \text{ kpc}$ , that is, within the solar circle, which seems to agree with the results obtained by Raboud et al. (1998) and Grenon (1999) for metal-rich stars. Other results may be seen in Table 9. All metal-rich barium stars lie inside in the  $(U,V)$ -plane of metal-rich stars of Raboud et al. (1998) and Grenon (1999), thus indicating that they display similar kinematical properties of non s-process enriched metal-rich

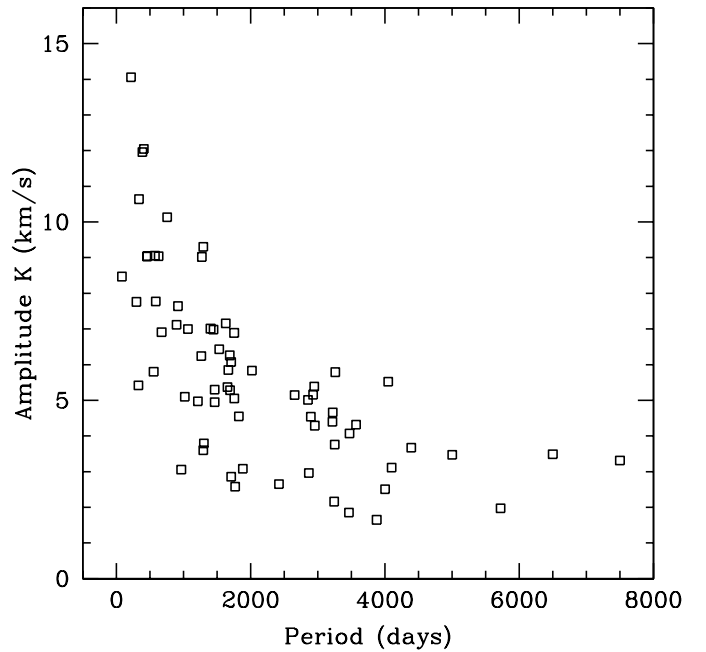


**Fig. 4.** Amplitude versus period for a sample of barium stars.

stars. Finally, the star HD 198590 with the highest  $Z_{max}$  value among the analyzed stars, with a metallicity of  $\approx+0.2$ , lies in the upper limit (with very few others) of the  $Z_{max}$  value in the  $Z_{max}$ -metallicity diagram of Grenon (1999). In Figure 13 of Soubiran & Girard (2005) this star lies between the thin-disk stars at  $([\text{Fe}/\text{H}], Z_{max})=(0.0, 0.1-0.2 \text{ kpc})$  and the thick-disk stars at  $([\text{Fe}/\text{H}], Z_{max})\approx(0.5, 1.0 \text{ kpc})$ . The other stars in Table 9 belong to the thin-disk stars with lower  $Z_{max}$  values.

#### 4.3. Abundances

In this section we compare the abundance ratios  $[\text{X}/\text{Fe}]$  of the metal-rich barium giants analyzed in this work with the results of some studies already made for giant stars. We used for comparison the data from local disk field giants studied by Luck & Heiter (2007), disk red-clump giants studied by Mishenina et al. (2006, 2007), metal-rich giants studied by Pakhomov et al. (2009) and two metal-rich open clusters and  $\mu$  Leo studied by Carretta et al. (2007). Figures 5 to 8 show the  $[\text{X}/\text{Fe}]$  ratios with metallicity for the barium giants of our sample and the results for the non s-process enriched giant stars mentioned above. We will see that with respect to the sodium, aluminum,  $\alpha$ -elements, chromium and nickel, the abundance ratios follow the same trend as seen in the disk-giant stars. For the heavy-elements, the  $[\text{s}/\text{Fe}]$  ratio, where 's' means the mean abundance of the elements synthesized by s-process, ranges from  $+0.2$  to  $+1.2$ , thus indicating different degrees of enhancements.

##### 4.3.1. Sodium to nickel

Sodium and aluminum are mainly produced by hydrostatic carbon burning in massive stars (Woosley & Weaver, 1995). Sodium and aluminum in disk stars has been observed among others by Edvardsson et al. (1993) and Feltzing & Gustafsson (1998). Over the range  $-1.0 < [\text{Fe}/\text{H}] < 0.0$ , the ratios  $[\text{Na}/\text{Fe}]$  and  $[\text{Al}/\text{Fe}]$  are slightly enhanced by  $\approx 0.1 \text{ dex}$ . For metal-rich stars Edvardsson et al. (1993) and Feltzing & Gustafsson (1998)

**Table 9.** Space velocities and Galactic orbital parameters for some metal-rich barium stars.

star	$U_{LSR}$ km s <sup>-1</sup>	$V_{LSR}$ km s <sup>-1</sup>	$W_{LSR}$ km s <sup>-1</sup>	$R_{min}$ kpc	$R_{max}$ kpc	$Z_{max}$ kpc	$e$
HD 46040	-2.3	-2.2	-15.0	7.19	7.95	0.3	0.05
HD 82765	9.5	-3.7	5.9	7.73	8.12	0.1	0.02
HD 100012	11.8	-5.1	4.1	7.53	8.10	0.1	0.04
HD 130386	-20.8	-25.0	13.7	6.46	8.35	0.3	0.13
HD 139660	5.5	-26.0	4.7	6.47	8.20	0.1	0.12
HD 198590	-14.9	2.8	26.3	7.97	8.72	0.6	0.05
HD 212209	50.6	20.0	-7.0	7.60	10.37	0.4	0.15

(see also Shi et al., 2004) observed an upturn in the [Na/Fe] ratio for metal-rich stars, that is  $[\text{Na}/\text{Fe}] = +0.2$  at  $[\text{Fe}/\text{H}] = +0.2$ . Shi et al. (2004) argued that to explain this Na overabundance for the metal-rich stars, large amounts of sodium have been produced by NeNa cycle in the interiors of AGB stars. Figure 5 shows that both the local giants and the red clump giants exhibit the same trend as seen in dwarf stars. The barium giants of our sample follow the same trend. For aluminum the ratio  $[\text{Al}/\text{Fe}]$  is almost constant at  $\approx 0.1$  in the metallicity range  $-2.0$  to  $0.2$  (Carretta et al., 2002; Edvardsson et al., 1993; Feltzing & Gustafsson, 1998). The local giants and our data for the barium giants seem to follow the same trend as seen for all these previous studies.

In the thick- and thin-disk stars the  $\alpha$ -element abundances given by the mean of Mg, Si, Ca, and Ti are overabundant by  $\approx 0.2$  dex at  $-1.0 < [\text{Fe}/\text{H}] < -0.5$  and then decrease by 0.1-0.0 dex at  $-0.5 < [\text{Fe}/\text{H}] < 0.0$  (Edvardsson et al., 1993; Reddy et al., 2003, 2006). Feltzing & Gustafsson (1998) observed that  $[\alpha/\text{Fe}]$  ratio has the same trend as detected by the other authors at  $-0.5 < [\text{Fe}/\text{H}] < 0.0$ . Up to  $[\text{Fe}/\text{H}] = +0.3$  the  $[\alpha/\text{Fe}]$  ratio remains flat at  $[\text{Fe}/\text{H}] = 0.0$ -0.1. The analysis of the local disk field giants studied by Luck & Heiter (2007) and disk red-clump giants studied by Mishenina et al. (2006) showed that giants display the same trend as mentioned above for the dwarfs. Figure 6 shows that the  $[\alpha/\text{Fe}]$  ratio versus  $[\text{Fe}/\text{H}]$  for the barium stars follows the same trend as the giants. The ratios  $[\text{X}/\text{Fe}]$  for the  $\alpha$ -elements, Mg, Si, Ca, and Ti are discussed below.

Magnesium (like oxygen) is produced in massive stars at  $\approx 25 \text{ M}_\odot$  as predicted by the nucleosynthesis theory (Woosley & Weaver, 1995) and iron is mainly produced by SNeI events. It would be expected that both ratios,  $[\text{O}/\text{Fe}]$  and  $[\text{Mg}/\text{Fe}]$ , would decrease with increasing metallicity. Indeed, the  $[\text{O}/\text{Fe}]$  ratio at  $[\text{Fe}/\text{H}] = -1.0$  is  $\approx +0.4$ , while at  $[\text{Fe}/\text{H}] = 0.2$  is  $\approx -0.1$  (Edvardsson et al., 1993). In halo stars, the  $[\text{Mg}/\text{Fe}]$  ratio also increases (like oxygen) toward lower metallicities (Norris et al., 2001). In dwarf disk stars, for metallicities higher than  $[\text{Fe}/\text{H}] > -0.2$  and up to  $+0.2$ , the ratio  $[\text{Mg}/\text{Fe}]$  becomes flat at  $\approx 0.1$  (Feltzing & Gustafsson, 1998; Chen et al., 2000). This observed trend of the  $[\text{Mg}/\text{Fe}]$  ratio toward the higher metallicities would suggest that Mg would not only be produced by massive stars but also by type I SNe events (Chen et al., 2000). Timmes et al. (1995) predict subsolar values for the  $[\text{Mg}/\text{Fe}]$  ratio at higher metallicities for the evolution of the magnesium abundances in the Galaxy, which is not seen in all the analysis of the  $[\text{Mg}/\text{Fe}]$  ratio. The analysis of the  $[\text{Mg}/\text{Fe}]$  ratio of local giants by Luck & Heiter (2007) as well as the barium giants of our sample shows the same trend as seen in dwarfs for metallicities higher than  $[\text{Fe}/\text{H}] > 0.0$  (Figure 5). However, the  $[\text{Mg}/\text{Fe}]$  ratio for the red clump giants analyzed by Mishenina et al. (2006) behaves like the  $[\text{O}/\text{Fe}]$  ratio.

Silicon can be produced by  $10 stars by hydrostatic oxygen burning and also during the eventual type$

II supernovae explosion (Woosley & Weaver, 1986). In halo stars at  $[\text{Fe}/\text{H}] = -3.0$  it is enhanced by  $\approx +0.5$  with larger scatter (Norris et al., 2001; Carretta et al., 2002). For dwarfs with metallicities higher than  $[\text{Fe}/\text{H}] = 0.0$ , it seems that silicon behaves like magnesium and has a  $[\text{Si}/\text{Fe}]$  ratio of  $\approx 0.05$  (Edvardsson et al., 1993). Inspecting the results of Feltzing & Gustafsson (1998), one can note that silicon flattens at a mean ratio of  $[\text{Si}/\text{Fe}] = 0.0$  for  $[\text{Fe}/\text{H}] = 0.0$ -0.4. For the red clump giants, the local giants and the barium giants analyzed in this work the relative-to-iron silicon abundance flattens at a mean ratio of  $[\text{Si}/\text{Fe}] \approx 0.1$  for  $[\text{Fe}/\text{H}] = 0.0$ -0.3.

Calcium shares the same nucleosynthesis site as silicon. In halo stars it is enhanced by 0.2-0.3 dex (Norris et al., 2001). In dwarfs and for metallicities higher than  $[\text{Fe}/\text{H}] > -0.2$ , calcium flattens toward a mean ratio  $[\text{Ca}/\text{Fe}]$  of  $\approx 0.0$ . The same trend is seen in barium and red clump giants but for the local giants, the  $[\text{Ca}/\text{Fe}]$  ratio is lower by -0.2 dex at  $[\text{Fe}/\text{H}] = +0.2$  (Luck & Heiter, 2007).

Titanium is usually considered an  $\alpha$ -element that is produced by explosive oxygen burning but could also be produced by Type Ia supernovae (Woosley & Weaver, 1995). Observationally, it behaves like an  $\alpha$ -element. Indeed, the  $[\text{Ti}/\text{Fe}]$  ratio for halo stars displays a similar trend as the  $[\text{Ca}/\text{Fe}]$  ratio. In dwarf-disk stars  $[\text{Ti}/\text{Fe}]$  slightly decreases with increasing metallicity (Edvardsson et al., 1993). For higher metallicities it seems that the ratio  $[\text{Ti}/\text{Fe}]$  flattens around  $\approx 0.1$ . In the present work, the  $[\text{Ti}/\text{Fe}]$  ratios are usually lower than the  $[\text{Mg}, \text{Si}, \text{Ca}/\text{Fe}]$  ratios, displaying a similar trend as local-disk giants (Luck & Heiter, 2007).

The iron peak elements are formed in large amounts in Type Ia supernovae and all its members should follow the same trend with iron abundance, therefore the  $[\text{X}/\text{Fe}]$  ratios should remain constant within the range of metallicity studied. Indeed, nickel, does remain constant with  $[\text{Ni}/\text{Fe}] = 0.0$  for  $-0.8 < [\text{Fe}/\text{H}] < 0.1$ . Luck & Heiter (2007) also found a tight correlation between  $[\text{Fe}/\text{H}]$  and  $[\text{Ni}/\text{H}]$  with a slope of 1.04 also between  $-0.8 < [\text{Fe}/\text{H}] < 0.1$ . However, some studies show a possible upturn after  $[\text{Fe}/\text{H}] > 0.1$  for red clump giants (Mishenina et al., 2006; Liu et al., 2007) and dwarfs (Chen et al., 2000). This upturn is seen in Luck & Heiter's data and also in Figure 4 of Soubiran & Girard (2005). For the element chromium, the study for the local giants of Luck & Heiter (2007) found a tight correlation between  $[\text{Fe}/\text{H}]$  and  $[\text{Cr}/\text{H}]$  with a slope of 1.06, that is  $[\text{Cr}/\text{Fe}] = 0.0$  for  $-0.8 < [\text{Fe}/\text{H}] < 0.2$ , despite some discrepant points, as they reported. The barium stars of our sample also follow the general trend seen for the field giants, for the ratios of  $[\text{Ni}/\text{Fe}]$  and  $[\text{Cr}/\text{Fe}]$ .

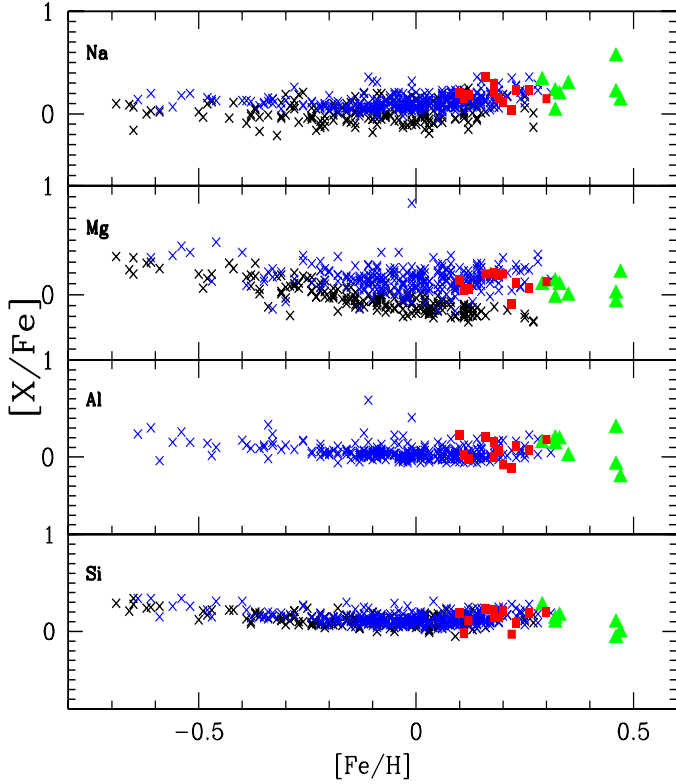


**Fig. 5.** Abundance ratios  $[X/\text{Fe}]$  vs.  $[\text{Fe}/\text{H}]$ . Metal-rich barium stars red squares; field giants of Luck & Heiter (2007), blue crosses; clump giants of Mishenina et al. (2006), black crosses; metal-rich giants stars and two metal-rich open clusters and  $\mu$  Leo studied by Pakhomov et al. (2009) and Carretta et al. (2007), respectively, green triangles.

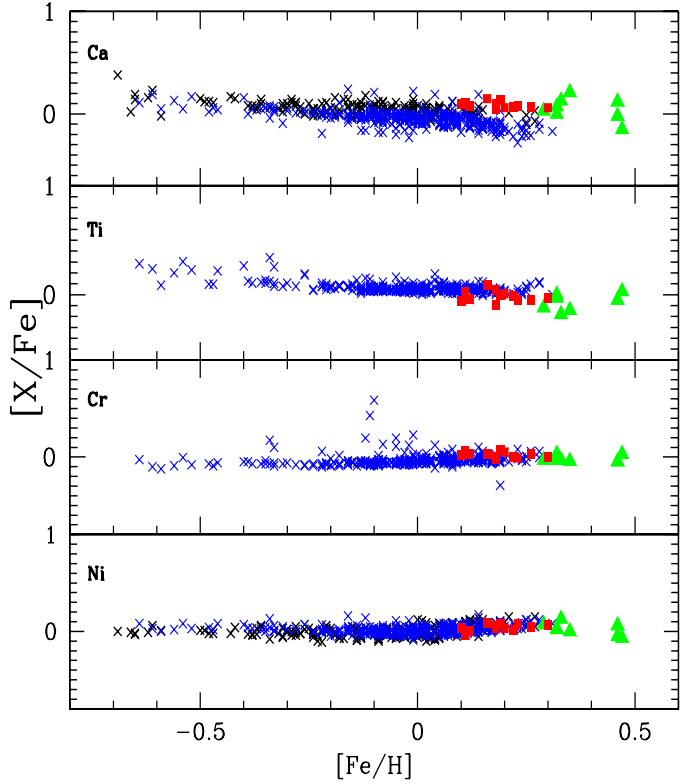


**Fig. 7.** Abundance ratios  $[X/\text{Fe}]$  vs.  $[\text{Fe}/\text{H}]$ . Symbols have the same meaning as in Fig. 5

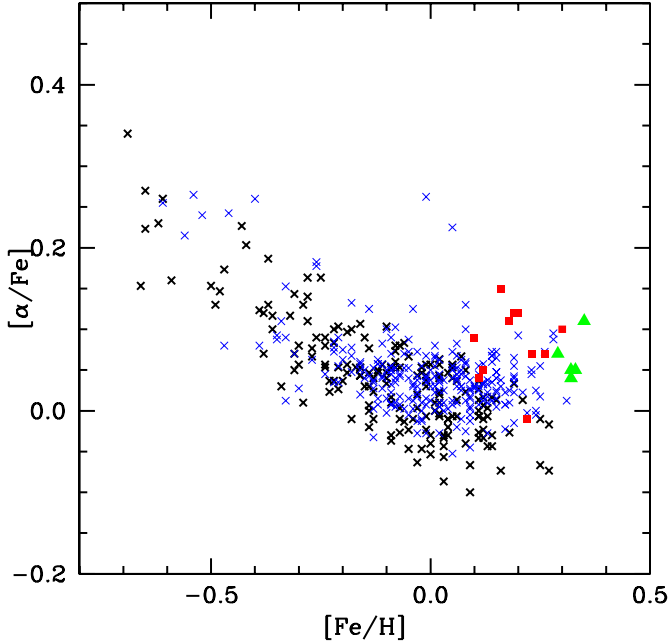
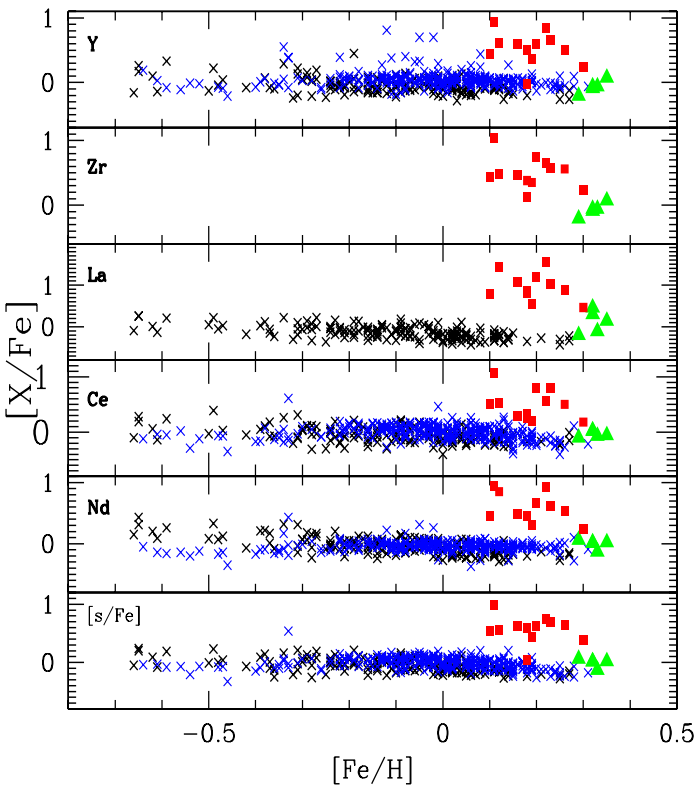


**Fig. 6.** Abundance ratios  $[\alpha/\text{Fe}]$  vs.  $[\text{Fe}/\text{H}]$ . Symbols have the same meaning as in Fig. 5

#### 4.3.2. s-process elements : Y, Zr, La, Ce and Nd

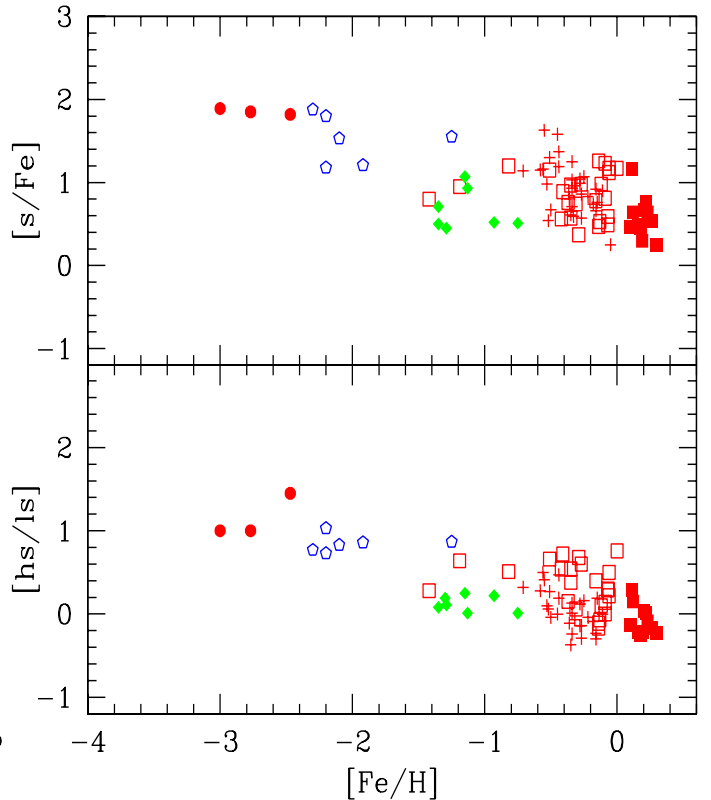
The main site of *s*-process elements (and also carbon) production are low-mass AGB stars ( $M \leq 3.0 M_{\odot}$ ) during the thermally pulsing phase (TP-AGB). Nucleosynthesis of *s*-process takes place in the C-rich intershell convective zone, the zone between the H-burning shell and the He-burning shell, of which the source of neutrons for the *s*-process to occur is the  $^{13}\text{C}(\alpha, n)^{16}\text{O}$  reaction (Lattanzio & Wood, 2003). Figure 8 shows the ratio  $[\text{s}/\text{Fe}]$ , where 's' represents the mean of the elements created by slow neutron capture reactions (*s*-process): Y, Zr, La, Ce, and Nd. As we can see from Figure 8, all stars except HD 100012 are enhanced in the *s*-process elements when compared to the same ratio of the field stars. HD 100012 has a  $[\text{s}/\text{Fe}]$  ratio of +0.22 and therefore cannot be considered as a barium star because some stars at this metallicity have a similar  $[\text{s}/\text{Fe}]$  ratio as HD 157919 with  $[\text{s}/\text{Fe}] = +0.2$  at  $[\text{Fe}/\text{H}] = +0.14$ . Among the local giants analyzed by Luck & Heiter (2007), only one barium star was spotted, HD 104979 (Zacs, 1994), which can be seen at  $[\text{Fe}/\text{H}] = -0.33$  with  $[\text{s}/\text{Fe}] = +0.54$ .

Figure 8 also shows that our sample stars differs from the field stars only by the degree of *s*-process enrichment observed in their atmospheres. Models of galactic chemical evolution do not predict this enrichment at this metallicity (Travaglio et al., 1999, 2004). Therefore, the atmospheres of these stars were contaminated either through the stellar evolution or an extrinsic event that may have happened in the past, i.e., mass-transfer hypothesis. The first hypothesis can be ruled out because of their position in the  $\log g$  -  $\log T_{\text{eff}}$  diagram (Figure 2). Finally, Figure 8 also shows that the abundance of zirconium is poorly investigated in normal giant stars in this metallicity range.



**Fig. 8.** Abundance ratios  $[X/\text{Fe}]$  vs.  $[\text{Fe}/\text{H}]$ . Symbols have the same meaning as in Fig. 5. Clump giants are from Mishenina et al. (2007).

Figure 9 shows the  $[\text{s}/\text{Fe}]$  ratios for chemically peculiar binary systems including not only the barium stars (giants and dwarfs) but also the yellow symbiotic stars, the CH stars, and the CEMP (carbon enhanced metal-poor) stars, those that have already been proved as binary systems. The definition of ‘s’ varies from author to author and in some cases depends on the quality and/or on the wavelength range of the available spectra. Among CEMP stars, there are six that are binaries: CS 22942-019, CS 22948-027, CS 29497-030, CS 29497-034, CS 22964-161, and HE 0024-2523, the data of which concerning their carbon and heavy-element ( $Z > 56$ ) overabundances and binarity were taken from the results of Preston & Sneden (2001); Sivarani et al. (2004); Barbuy et al. (2005); Lucatello et al. (2003); Thompson et al. (2008); Aoki et al. (2002) and Hill et al. (2000). According to the mass-transfer hypothesis for the origin of the barium stars, one of the binary components ejects its envelope that is enriched in the s-process elements produced during the AGB phase, and this matter falls onto the companion, which in turn becomes enriched in these elements, and now is the barium star. The different ratios  $[\text{s}/\text{Fe}]$  observed among the barium stars, also seen in this study, depend on the material received by the companion as well as whether this material is partially or fully mixed in the atmosphere of the barium stars. Theoretical studies for the production of the s-process elements in intrinsic AGB stars (Gallino et al., 1998; Busso et al., 1999) indicate that there is a trend that the s-process elements are more easily produced at lower metallicities as a result of the operation of the reaction  $^{13}\text{C}(\alpha, \text{n})^{16}\text{O}$  as a neutron source. When several classes of



**Fig. 9.** Diagram of  $[\text{s}/\text{Fe}]$  versus  $[\text{Fe}/\text{H}]$  (top) and  $[\text{hs}/\text{ls}]$  versus  $[\text{Fe}/\text{H}]$  (bottom) for several classes of chemically peculiar binary stars. Metal-rich barium stars (filled red squares); barium giants previously analyzed (red open squares); barium dwarfs (plus red crosses); CH stars (blue open polygons); yellow symbiotic (green symbols) and CEMP-s stars which are members of binary systems (red filled circles)

chemically-peculiar stars are examined all together (Figure 9), this phenomenon is observed.

According to Busso et al. (1999) and Travaglio et al. (2004), the neutron-capture nucleosynthesis in AGB stars is metallicity-dependent. Among the elements created by the s-process nucleosynthesis, the first neutron magic peak elements (such as Y and Zr) are the dominant products of the neutron captures in AGB models at metallicities around  $[\text{Fe}/\text{H}] = -0.4$ . At lower metallicities,  $[\text{Fe}/\text{H}] \approx -1.0$ , the second neutron magic peak elements (Ba-La-Ce-Nd) are the dominant. The origin of these two peaks is the result of the neutron magic numbers 50 and 82 nuclei, which have smaller absorption cross-sections than their neighbor nuclei and therefore turn out to be more stable than others. Owing to this, it is possible to monitor the s-process efficiency through the relative abundances of the second-peak elements to the first-peak elements. In this way the s-elements at the second-peak are usually referred to as the “heavy” s-process elements, in our case, La, Ce, and Nd, while s-elements at the first-peak are usually referred to as the “light” elements, in our case, Y and Zr. Thus, the average logarithmic ratio  $[\text{hs}/\text{ls}]$  has been widely used to measure the efficiency of neutron captures. Table 10 provides the ratios  $[\text{ls}/\text{Fe}]$ ,  $[\text{hs}/\text{Fe}]$  as well as the ratio  $[\text{hs}/\text{ls}]$  for the studied stars. Inspecting Table 10, we see that our derived values for the indices  $[\text{hs}/\text{ls}]$ ,  $[\text{hs}/\text{Fe}]$ ,  $[\text{ls}/\text{Fe}]$  for all metal-rich barium stars, except for HD 46040, are in the range,  $-0.3$  to  $0.0$ ,  $0.2$  to  $0.7$  and  $0.4$  to  $0.8$ . These values seem to agree well when compared with

**Table 10.** Indices of the s-process.

star	[ls/Fe]	[hs/Fe]	[hs/ls]
CD-25 6606	0.55	0.70	0.15
HD 46040	0.99	1.28	0.29
HD 49841	0.75	0.76	0.01
HD 82765	0.43	0.22	-0.21
HD 84734	0.62	0.66	0.04
HD 85205	0.70	0.61	-0.09
HD 101079	0.54	0.41	-0.13
HD 130386	0.62	0.41	-0.21
HD 139660	0.64	0.47	-0.17
HD 198590	0.60	0.35	-0.25
HD 212209	0.39	0.16	-0.23

model predictions given by Busso et al. (2001) as seen in their Figures 7, 8, and 9 for the ratios [hs/ls], [hs/Fe], [ls/Fe] vs metallicity for the standard case (ST/1.5). The ST case corresponds to  $4 \times 10^{-6} M_{\odot}$  of  $^{13}\text{C}$  for AGB stars between 1.5 and  $3.0 M_{\odot}$  for a metallicity of  $[\text{Fe}/\text{H}] = -0.3$ , which accounts for the main component of the s-process in solar system (Busso et al., 2001). HD 46040 has higher values for the indices [hs/ls] and [hs/Fe] for a star at this metallicity and its [ls/Fe] index marginally falls in the limit of the model predictions.

In Figure 9 we show the [hs/ls] index as a function of the metallicity for the same classes of chemically peculiar binary systems. As for the [s/Fe] ratio vs metallicity, the [hs/ls] index also increases toward lower metallicities, with a large spread. In both figures we can see that the position of metal-rich barium stars are useful targets for constraining models for the nucleosynthesis of the s-process at higher metallicities.

## 5. Conclusions

Our abundance analysis has been performed by employing high-resolution optical spectra of a sample of metal-rich barium stars with the aim to obtain their abundance pattern and kinematical properties, and it can be summarized as follows:

1. The stars have enhancement factors, [s/Fe], from 0.25 up to 1.16. These overabundances are expected for stars at this metallicity according to the models of Busso et al. (2001), which are based on the observed indices [ls/Fe], [hs/Fe] and [hs/ls]. The abundance pattern of the iron peak elements, of the elements of the  $\alpha$  group, as well as that of sodium and aluminum follows the disk abundance. The [alpha/Fe] ratios in our stars do not show any trace of overabundances, while bulge stars display increased ratios (Lecureur et al., 2007). Therefore, these metal-rich barium stars do not belong to the bulge population. It is probable that like the most of the non s-process enriched metal-rich stars, the barium stars analyzed in this work belong to the thin-disk stars, as can be deduced from their low  $Z_{\max}$  values. Also interesting to note is that all stars analyzed in this work have low values for the eccentricities, which indicates almost circular orbits in agreement with this characteristic of the other non s-process enriched metal-rich stars previously analyzed (Pakhomov et al., 2009; Gratton & Sneden, 1990) and which agrees with the results of Raboud et al. (1998).
2. Considering evolutionary aspects, metal-rich barium stars put another constraint on the evolution of barium dwarfs to barium giants. Because all CH subgiants and barium dwarfs analyzed so far have metallicities less than the metallicity of the Sun, except those very few subgiants analyzed

in this paper, metal-rich barium dwarfs/subgiants are yet to be found. In this respect the same question can be addressed to the yellow symbiotics. All yellow symbiotics, except for the D'-type, which probably are not symbiotic stars (Corradi & Schwarz, 1997; Pereira, 2005), are halo objects and their connection with metal-poor barium stars have been investigated in the recent years (Smith et al., 1996, 1997; Jorissen et al., 2005; Pereira & Roig, 2009). Consequently, disk yellow symbiotics at near solar metallicity have not yet been identified.

3. Metal-rich barium stars are useful objects for investigating the heavy-element abundance pattern at metallicities higher than the metallicity of the Sun because they are free of many molecular features that are usually seen in the spectra of MS, S, and carbon stars. The barium star phenomenon once it extend toward higher metallicities, shares several properties with the non s-process enriched metal-rich and super metal-rich giant stars previously investigated.

*Acknowledgements.* This research has made use of the SIMBAD database, operated at CDS, Strasbourg, France. We thank our referee for detailed comments that have improved the presentation of the present work.

## References

- Allen, D. M. & Barbuy, B. 2006, A&A, 454, 917
- Alonso, A., Arribas, S., & Martínez-Roger, C. 1999, A&AS, 140, 261
- Antipova, L. I., Boyarchuk, A. A., Pakhomov, Y. V., & Panchuk, V. E. 2003, Astronomy Reports, 47, 648
- Antipova, L. I., Boyarchuk, A. A., Pakhomov, Y. V., & Panchuk, V. E. 2004, Astronomy Reports, 48, 597
- Aoki, W., Ryan, S. G., Norris, J. E., et al. 2002, ApJ, 580, 1149
- Arp, H. 1965, ApJ, 141, 43
- Barbuy, B. & Grenon, M. 1990, in European Southern Observatory Conference and Workshop Proceedings, Vol. 35, European Southern Observatory Conference and Workshop Proceedings, ed. B. J. Jarvis & D. M. Terndrup, 83–86
- Barbuy, B., Spite, M., Spite, F., et al. 2005, A&A, 429, 1031
- Bessell, M. S., Castelli, F., & Plez, B. 1998, A&A, 333, 231
- Bidelman, W. P. 1981, AJ, 86, 553
- Biemont, E., Grevesse, N., Hannaford, P., & Lowe, R. M. 1981, ApJ, 248, 867
- Busso, M., Gallino, R., Lambert, D. L., Travaglio, C., & Smith, V. V. 2001, ApJ, 557, 802
- Busso, M., Gallino, R., & Wasserburg, G. J. 1999, ARA&A, 37, 239
- Carretta, E., Bragaglia, A., & Gratton, R. G. 2007, A&A, 473, 129
- Carretta, E., Gratton, R., Cohen, J. G., Beers, T. C., & Christlieb, N. 2002, AJ, 124, 481
- Castro, S., Rich, R. M., Grenon, M., Barbuy, B., & McCarthy, J. K. 1997, AJ, 114, 376
- Cayrel, R. 1988, in IAU Symposium, Vol. 132, The Impact of Very High S/N Spectroscopy on Stellar Physics, ed. G. Cayrel de Strobel & M. Spite, 345
- Chen, Y. Q., Nissen, P. E., Zhao, G., Zhang, H. W., & Benoni, T. 2000, A&AS, 141, 491
- Corradi, R. & Schwarz, H. E. 1997, in Physical Processes in Symbiotic Binaries and Related Systems, ed. J. Mikolajewska, 147
- Drake, J. J. & Smith, G. 1991, MNRAS, 250, 89
- Drake, N. A. & Pereira, C. B. 2008, AJ, 135, 1070
- Edvardsson, B., Andersen, J., Gustafsson, B., et al. 1993, A&A, 275, 101
- Eggen, O. J. 1993, AJ, 106, 80
- Feltzing, S. & Gustafsson, B. 1998, A&AS, 129, 237
- Gallino, R., Arlandini, C., Busso, M., et al. 1998, ApJ, 497, 388
- Girardi, L., Bressan, A., Bertelli, G., & Chiosi, C. 2000, A&AS, 141, 371
- Gomez, A. E., Luri, X., Grenier, S., et al. 1997, A&A, 319, 881
- Gratton, R. G. & Sneden, C. 1988, A&A, 204, 193
- Gratton, R. G. & Sneden, C. 1990, A&A, 234, 366
- Grenon, M. 1972, in IAU Colloq. 17: Age des Etoiles, ed. G. Cayrel de Strobel & A. M. Delplace, 55
- Grenon, M. 1999, Ap&SS, 265, 331
- Han, Z., Eggleton, P. P., Podsiadlowski, P., & Tout, C. A. 1995, MNRAS, 277, 1443
- Hannaford, P., Lowe, R. M., Grevesse, N., Biemont, E., & Whaling, W. 1982, ApJ, 261, 736
- Hill, V., Andrievsky, S., & Spite, M. 1995, A&A, 293, 347

- Hill, V., Barbuy, B., Spite, M., et al. 2000, A&A, 353, 557  
 Johnson, D. R. H. & Soderblom, D. R. 1987, AJ, 93, 864  
 Jorissen, A. & Mayor, M. 1988, A&A, 198, 187  
 Jorissen, A., Začs, L., Udry, S., Lindgren, H., & Musaev, F. A. 2005, A&A, 441, 1135  
 Junqueira, S. & Pereira, C. B. 2001, AJ, 122, 360  
 Kaufer, A., Stahl, O., Tubbesing, S., et al. 1999, The Messenger, 95, 8  
 Lambert, D. L., Heath, J. E., Lemke, M., & Drake, J. 1996, ApJS, 103, 183  
 Lattanzio, J. C. & Wood, P. R. 2003, Evolution, Nucleosynthesis and Pulsations of AGB stars., ed. H. J. Habing & H. Olofsson  
 Lecureur, A., Hill, V., Zoccali, M., et al. 2007, A&A, 465, 799  
 Liu, Y. J., Zhao, G., Shi, J. R., Pietrzynski, G., & Gieren, W. 2007, MNRAS, 382, 553  
 Lucatello, S., Gratton, R., Cohen, J. G., et al. 2003, AJ, 125, 875  
 Luck, R. E. & Bond, H. E. 1991, ApJS, 77, 515  
 Luck, R. E. & Heiter, U. 2007, AJ, 133, 2464  
 MacConnell, D. J., Frye, R. L., & Upgren, A. R. 1972, AJ, 77, 384  
 Martin, G. A., Fuhr, J. R., & Wiese, W. L. 1988, Atomic transition probabilities. Scandium through Manganese, ed. Martin, G. A., Fuhr, J. R., & Wiese, W. L.  
 Martin, W., Fuhr, J., Kelleher, D., et al. 2002, NIST Atomic Spectra Database Version2.0 (Online Available), NIST Standard Reference Database, National Institute of Standards and Technology, Gaithersburg Maryland  
 Matteucci, F. 2003, The Chemical Evolution of the Galaxy, ed. Matteucci, F.  
 McWilliam, A. & Rich, R. M. 1994, ApJS, 91, 749  
 Mennessier, M. O., Luri, X., Figueras, F., et al. 1997, A&A, 326, 722  
 Mishenina, T. V., Bienaymé, O., Gorbaneva, T. I., et al. 2006, A&A, 456, 1109  
 Mishenina, T. V., Gorbaneva, T. I., Bien aymé, O., et al. 2007, Astronomy Reports, 51, 382  
 Norris, J. E., Ryan, S. G., & Beers, T. C. 2001, ApJ, 561, 1034  
 Pakhomov, Y. V., Antipova, L. I., Boyarchuk, A. A., Zhao, G., & Liang, Y. 2009, Astronomy Reports, 53, 685  
 Pereira, C., Roig, F., Chavero, C., & et al. 2011, in prep.  
 Pereira, C. B. 2005, AJ, 129, 2469  
 Pereira, C. B. & Drake, N. A. 2009, A&A, 496, 791  
 Pereira, C. B. & Drake, N. A. 2011, AJ, 141, 79  
 Pereira, C. B. & Roig, F. 2009, AJ, 137, 118  
 Perryman, M. A. C. & ESA, eds. 1997, ESA Special Publication, Vol. 1200, The HIPPARCOS and TYCHO catalogues. Astrometric and photometric star catalogues derived from the ESA HIPPARCOS Space Astrometry Mission  
 Preston, G. W. & Sneden, C. 2001, AJ, 122, 1545  
 Raboud, D., Grenon, M., Martinet, L., Fux, R., & Udry, S. 1998, A&A, 335, L61  
 Reddy, B. E., Lambert, D. L., & Allende Prieto, C. 2006, MNRAS, 367, 1329  
 Reddy, B. E., Tomkin, J., Lambert, D. L., & Allende Prieto, C. 2003, MNRAS, 340, 304  
 Reyniers, M., Van Winckel, H., Gallino, R., & Straniero, O. 2004, A&A, 417, 269  
 Schaefer, D., Charbonnel, C., Meynet, G., Maeder, A., & Schaller, G. 1993, A&AS, 102, 339  
 Schönrich, R., Binney, J., & Dehnen, W. 2010, MNRAS, 403, 1829  
 Shi, J. R., Gehren, T., & Zhao, G. 2004, A&A, 423, 683  
 Sivarani, T., Bonifacio, P., Molaro, P., et al. 2004, A&A, 413, 1073  
 Smiljanic, R., Porto de Mello, G. F., & da Silva, L. 2007, A&A, 468, 679  
 Smith, G., Edwardsson, B., & Frisk, U. 1986, A&A, 165, 126  
 Smith, V. V., Coleman, H., & Lambert, D. L. 1993, ApJ, 417, 287  
 Smith, V. V., Cunha, K., Jorissen, A., & Boffin, H. M. J. 1996, A&A, 315, 179  
 Smith, V. V., Cunha, K., Jorissen, A., & Boffin, H. M. J. 1997, A&A, 324, 97  
 Smith, V. V., Pereira, C. B., & Cunha, K. 2001, ApJ, 556, L55  
 Smith, V. V. & Suntzeff, N. B. 1987, AJ, 93, 359  
 Sneden, C., McWilliam, A., Preston, G. W., et al. 1996, ApJ, 467, 819  
 Sneden, C. A. 1973, PhD thesis, THE UNIVERSITY OF TEXAS AT AUSTIN.  
 Soubiran, C. & Girard, P. 2005, A&A, 438, 139  
 Spinrad, H. & Taylor, B. J. 1969, ApJ, 157, 1279  
 Thompson, I. B., Ivans, I. I., Bisterzo, S., et al. 2008, ApJ, 677, 556  
 Timmes, F. X., Woosley, S. E., & Weaver, T. A. 1995, ApJS, 98, 617  
 Travaglio, C., Galli, D., Gallino, R., et al. 1999, ApJ, 521, 691  
 Travaglio, C., Gallino, R., Arnone, E., et al. 2004, ApJ, 601, 864  
 Udry, S., Jorissen, A., Mayor, M., & Van Eck, S. 1998a, A&AS, 131, 25  
 Udry, S., Mayor, M., Van Eck, S., et al. 1998b, A&AS, 131, 43  
 Van Winckel, H. & Reyniers, M. 2000, A&A, 354, 135  
 Wiese, W. L., Smith, M. W., & Miles, B. M. 1969, Atomic transition probabilities. Vol. 2: Sodium through Calcium. A critical data compilation, ed. Wiese, W. L., Smith, M. W., & Miles, B. M.  
 Woosley, S. E. & Weaver, T. A. 1986, ARA&A, 24, 205  
 Woosley, S. E. & Weaver, T. A. 1995, ApJS, 101, 181  
 Zacs, L. 1994, A&A, 283, 937

**Table 2.** Observed Fe I and Fe II lines.

Element	$\lambda(\text{\AA})$	$\chi(\text{eV})$	$\log gf$	Equivalent Widths (m\AA)							
				CD	HD	HD	HD	HD	HD	HD	HD
Fe I	5242.49	3.63	-0.970	118	125	113	127	127	137	134	
	5253.03	2.28	-3.790	—	—	—	60	—	57	72	
	5288.52	3.69	-1.510	93	—	—	—	99	118	—	
	5315.05	4.37	-1.400	69	—	—	—	—	93	—	
	5321.11	4.43	-1.190	—	92	67	—	76	82	72	
	5322.04	2.28	-2.840	111	125	109	110	114	133	—	
	5373.71	4.47	-0.710	89	—	—	—	92	102	96	
	5389.48	4.42	-0.250	104	112	—	—	112	—	—	
	5417.03	4.42	-1.530	57	—	62	68	68	81	71	
	5441.34	4.31	-1.580	57	—	—	73	70	70	69	
	5445.04	4.39	0.040	136	—	—	—	—	—	—	
	5522.45	4.21	-1.400	69	—	—	—	—	—	—	
	5560.21	4.43	-1.040	79	81	71	—	78	—	84	
	5567.39	2.61	-2.560	116	—	—	—	—	—	—	
	5624.02	4.39	-1.330	—	—	—	—	—	101	86	
	5633.95	4.99	-0.120	86	—	—	95	—	108	101	
	5635.82	4.26	-1.740	40	65	57	64	62	58	66	
	5638.26	4.22	-0.720	97	—	102	114	111	115	119	
	5691.50	4.30	-1.370	69	—	—	—	—	90	—	
	5705.47	4.30	-1.360	52	72	65	75	67	73	77	
	5717.83	4.28	-0.979	—	107	95	—	—	—	—	
	5731.76	4.26	-1.150	87	106	91	93	97	105	99	
	5806.73	4.61	-0.900	74	87	82	85	86	89	93	
	5814.81	4.28	-1.820	38	56	45	50	54	54	56	
	5852.22	4.55	-1.180	65	—	69	76	78	86	88	
	5855.09	4.61	-1.520	—	—	—	49	—	—	—	
	5856.10	4.29	-1.550	—	—	—	62	—	—	—	
	5862.35	4.55	-0.390	—	—	—	112	—	—	—	
	5883.82	3.96	-1.210	95	—	—	112	101	116	—	
	5916.25	2.45	-2.990	97	—	—	—	—	—	—	
	5934.65	3.93	-1.020	110	—	105	107	112	123	119	
	6024.06	4.55	-0.060	133	—	136	—	—	—	—	
	6027.05	4.08	-1.090	91	106	87	100	—	110	103	
	6054.07	4.37	-2.310	—	—	—	—	—	31	—	
	6056.01	4.73	-0.400	91	97	—	99	96	100	103	
	6078.50	4.80	-0.340	—	—	—	105	—	—	—	
	6079.01	4.65	-0.970	68	—	70	75	76	79	82	
	6082.71	2.22	-3.580	—	—	80	—	—	—	—	
	6093.64	4.61	-1.350	—	—	54	54	66	63	65	
	6094.37	4.65	-1.940	—	—	39	—	—	—	—	
	6096.66	3.98	-1.780	—	75	63	70	68	74	75	
	6120.25	0.91	-5.950	21	64	33	—	32	40	51	
	6151.62	2.18	-3.290	87	117	95	105	100	111	108	
	6157.73	4.08	-1.110	105	—	—	—	—	123	118	
	6165.36	4.14	-1.470	68	80	73	78	82	88	83	
	6173.34	2.22	-2.880	115	—	114	130	—	—	—	
	6180.20	2.73	-2.650	—	—	98	—	—	—	—	
	6187.99	3.94	-1.570	73	98	83	91	88	85	92	
	6200.31	2.60	-2.440	112	—	118	123	126	—	133	
	6213.43	2.22	-2.480	126	—	—	—	—	—	—	
	6253.83	4.73	-1.660	—	—	39	—	—	—	—	
	6315.81	4.07	-1.710	—	—	72	—	—	—	—	
	6322.69	2.59	-2.430	117	—	124	132	—	—	135	
	6380.74	4.19	-1.320	—	—	89	—	98	102	104	
	6419.95	4.73	-0.090	—	—	111	—	—	—	—	
	6436.41	4.19	-2.460	27	—	39	37	—	—	41	
	6469.19	4.83	-0.620	93	—	97	—	100	—	—	
	6496.47	4.79	-0.570	—	—	89	—	—	—	—	
	6498.95	0.96	-4.630	—	—	—	121	—	—	—	



**Table 2.** Observed Fe I and Fe II lines.

Element	$\lambda(\text{\AA})$	$\chi(\text{eV})$	$\log gf$	Equivalent Widths (m\AA)				
				HD 101079	HD 130386	HD 139660	HD 198590	HD 212209
Fe I	5242.49	3.63	-0.970	115	119	124	127	132
	5253.03	2.28	-3.790	63	—	74	—	—
	5288.52	3.69	-1.510	97	100	114	—	—
	5321.11	4.43	-1.190	67	76	78	74	84
	5322.04	2.28	-2.840	107	119	119	114	131
	5373.71	4.47	-0.710	86	87	91	94	95
	5389.48	4.42	-0.250	108	—	—	112	—
	5417.03	4.42	-1.530	64	—	71	72	77
	5441.34	4.31	-1.580	62	68	70	67	72
	5445.04	4.39	0.041	134	—	—	—	—
	5522.45	4.21	-1.400	—	—	80	—	87
	5531.98	4.91	-1.460	42	—	—	—	—
	5560.21	4.43	-1.040	74	77	78	83	83
	5584.77	3.57	-2.170	76	—	—	—	—
	5624.02	4.39	-1.330	83	—	92	91	—
	5633.95	4.99	-0.120	92	102	—	—	98
	5635.82	4.26	-1.740	60	64	67	60	69
	5638.26	4.22	-0.720	111	115	114	111	119
	5705.47	4.30	-1.360	67	72	75	70	81
	5717.83	4.28	-0.979	—	—	109	—	—
	5731.76	4.26	-1.150	92	100	95	92	103
	5806.73	4.61	-0.900	82	89	90	82	92
	5814.81	4.28	-1.820	47	53	58	48	61
	5852.22	4.55	-1.180	74	—	89	77	—
	5883.82	3.96	-1.210	105	105	104	104	103
	5916.25	2.45	-2.990	106	—	—	—	—
	5934.65	3.93	-1.020	108	117	116	116	125
	6027.05	4.08	-1.090	96	103	—	98	106
	6056.01	4.73	-0.400	95	—	100	102	104
	6079.01	4.65	-0.970	68	70	84	80	—
	6082.71	2.22	-3.580	—	—	—	93	—
	6093.64	4.61	-1.350	56	56	61	63	70
	6096.66	3.98	-1.780	68	75	75	69	78
	6120.25	0.91	-5.950	—	53	—	39	67
	6151.62	2.18	-3.290	97	108	109	102	119
	6157.73	4.08	-1.110	105	—	122	117	—
	6165.36	4.14	-1.470	74	77	81	80	85
	6173.34	2.22	-2.880	120	—	139	132	—
	6187.99	3.94	-1.570	80	90	91	89	105
	6200.31	2.60	-2.440	120	—	133	123	—
	6213.43	2.22	-2.480	136	—	—	—	—
	6322.69	2.59	-2.430	124	—	—	—	—
	6380.74	4.19	-1.320	92	103	—	100	—
	6436.41	4.19	-2.460	36	—	47	40	53
	6469.19	4.83	-0.620	96	—	—	103	—
	6518.37	2.83	-2.300	—	109	—	—	122
	6574.23	0.99	-5.020	—	107	—	95	130
	6591.31	4.59	-2.070	28	36	31	—	—
	6597.56	4.79	-0.920	69	74	73	74	82
	6608.03	2.28	-4.030	—	68	—	—	—
	6609.11	2.56	-2.690	125	—	—	—	—
	6646.93	2.61	-3.990	—	—	—	58	—
	6653.85	4.14	-2.520	27	34	41	29	39
	6699.14	4.59	-2.190	25	38	37	29	43
	6703.57	2.76	-3.160	—	—	—	100	—
	6704.48	4.22	-2.660	19	27	22	17	—
	6713.74	4.79	-1.600	41	—	52	47	56
	6739.52	1.56	-4.950	—	64	—	57	76
	6745.96	4.07	-2.770	—	22	23	21	35

	6752.71	4.64	-1.200	—	—	—	92	—
	6793.26	4.07	-2.470	33	—	46	—	51
	6806.85	2.73	-3.210	93	91	—	92	—
	6810.26	4.61	-0.990	75	85	88	83	92
	6820.37	4.64	-1.170	72	80	90	82	89
	6858.15	4.61	-0.930	81	93	89	86	—
Fe II	4993.35	2.81	-3.670	64	65	69	65	59
	5132.66	2.81	-4.000	48	—	59	66	—
	5197.56	3.23	-2.250	—	—	117	—	—
	5234.62	3.22	-2.240	112	110	107	119	103
	5284.10	2.89	-3.010	—	—	—	—	77
	5325.56	3.22	-3.170	63	61	—	73	66
	5414.05	3.22	-3.620	51	41	55	64	53
	5425.25	3.20	-3.210	66	57	61	76	—
	5991.37	3.15	-3.560	60	55	61	68	55
	6084.10	3.20	-3.800	46	43	47	60	—
	6149.25	3.89	-2.720	53	48	58	60	47
	6247.55	3.89	-2.340	—	—	69	—	59
	6416.92	3.89	-2.680	63	55	59	65	57
	6432.68	2.89	-3.580	69	63	65	82	59

**Table 4.** Other lines studied.

$\lambda(\text{\AA})$	Species	$\chi(\text{eV})$	$\log g f$	Ref	Equivalent widths (m\AA)						
					CD -25 6606	HD 46040	HD 49841	HD 82765	HD 84734	HD 85205	
5682.65	Na I	2.10	-0.700	PS	140	—	—	—	148	—	
5688.22	Na I	2.10	-0.400	PS	—	—	151	—	152	—	
6154.22	Na I	2.10	-1.510	R03	81	93	75	90	92	98	
6160.75	Na I	2.10	-1.210	R03	89	123	111	107	100	116	
4730.04	Mg I	4.34	-2.390	R03	—	—	—	—	104	—	
5711.10	Mg I	4.34	-1.750	R99	128	143	126	139	138	146	
6318.71	Mg I	5.11	-1.940	Ca07	65	84	64	84	—	77	
6319.24	Mg I	5.11	-2.160	Ca07	—	51	52	61	44	—	
6319.49	Mg I	5.11	-2.670	Ca07	—	30	15	39	—	—	
6965.41	Mg I	5.75	-1.720	MR94	41	71	64	71	75	69	
7387.70	Mg I	5.75	-0.870	MR94	81	—	—	118	—	119	
8712.69	Mg I	5.93	-1.260	E93	—	—	71	103	—	87	
8717.83	Mg I	5.91	-0.970	WSM	108	—	88	104	136	117	
8736.04	Mg I	5.94	-0.340	WSM	146	139	137	156	—	—	
6696.03	Al I	3.14	-1.481	MR94	—	79	59	77	59	—	
6698.67	Al I	3.14	-1.630	R03	38	78	54	56	51	—	
7835.32	Al I	4.04	-0.580	R03	64	—	62	80	64	91	
7836.13	Al I	4.02	-0.400	R03	69	91	79	95	77	95	
8772.88	Al I	4.02	-0.250	R03	100	108	101	102	125	—	
8773.91	Al I	4.02	-0.070	R03	123	—	103	135	—	—	
5793.08	Si I	4.93	-2.060	R03	69	—	—	83	78	90	
6125.03	Si I	5.61	-1.540	E93	51	—	52	57	58	59	
6131.58	Si I	5.62	-1.685	E93	—	37	38	54	—	56	
6145.02	Si I	5.61	-1.430	E93	58	47	52	61	57	68	
6155.14	Si I	5.62	-0.770	E93	104	97	97	115	114	112	
7760.64	Si I	6.20	-1.280	E93	42	18	25	36	61	39	
7800.00	Si I	6.18	-0.720	E93	—	—	59	83	100	100	
8728.01	Si I	6.18	-0.360	E93	105	—	85	106	—	105	
8742.45	Si I	5.87	-0.510	E93	114	88	111	124	121	137	
6161.30	Ca I	2.52	-1.270	E93	96	—	—	107	—	113	
6166.44	Ca I	2.52	-1.140	R03	99	116	105	110	115	110	
6169.04	Ca I	2.52	-0.800	R03	121	153	130	138	133	149	
6169.56	Ca I	2.53	-0.480	DS91	146	—	146	154	143	—	
6455.60	Ca I	2.51	-1.290	R03	89	125	104	108	103	114	
6471.66	Ca I	2.51	-0.690	S86	125	146	128	136	132	—	
4758.12	Ti I	2.25	0.425	MFK	75	—	75	—	—	—	
4759.28	Ti I	2.25	0.514	MFK	—	—	79	87	—	—	
4820.41	Ti I	1.50	-0.439	MFK	—	—	—	—	109	—	
4997.10	Ti I	0.00	-2.118	MFK	—	—	85	92	87	—	
5016.17	Ti I	0.85	-0.574	MFK	114	—	—	129	127	—	
5022.87	Ti I	0.83	-0.434	MFK	—	—	125	128	128	—	
5039.96	Ti I	0.02	-1.130	MFK	—	—	134	144	—	—	
5043.59	Ti I	0.84	-1.733	MFK	—	—	75	82	—	—	
5062.10	Ti I	2.16	-0.464	MFK	—	—	48	—	55	42	
5113.45	Ti I	1.44	-0.880	E93	60	91	63	72	61	—	
5145.47	Ti I	1.46	-0.574	MFK	72	112	83	86	85	86	
5152.19	Ti I	0.02	-2.024	MFK	—	—	86	—	92	—	
5219.71	Ti I	0.02	-2.292	MFK	—	—	95	99	93	91	
5223.63	Ti I	2.09	-0.559	MFK	43	74	53	54	44	41	
5295.78	Ti I	1.05	-1.633	MFK	40	79	48	54	51	55	
5490.16	Ti I	1.46	-0.937	MFK	—	—	—	—	71	66	
5662.16	Ti I	2.32	-0.109	MFK	—	86	—	77	74	74	
5689.48	Ti I	2.30	-0.469	MFK	39	66	40	58	41	51	
5866.46	Ti I	1.07	-0.871	E93	97	—	105	119	119	—	
5922.12	Ti I	1.05	-1.465	MFK	—	95	66	70	82	—	
5978.55	Ti I	1.87	-0.496	MFK	54	102	64	60	70	61	
6091.18	Ti I	2.27	-0.370	R03	38	—	51	59	51	53	
6126.22	Ti I	1.05	-1.370	R03	63	—	72	80	79	76	
6258.11	Ti I	1.44	-0.355	MFK	97	—	102	113	111	118	

6261.10	Ti I	1.43	-0.480	B86	94	—	112	121	108	119
6554.24	Ti I	1.44	-1.219	MFK	43	—	64	68	59	51
4789.34	Cr I	2.54	-0.365	MFK	—	—	120	—	—	—
4801.03	Cr I	3.12	-0.130	MFK	84	—	83	100	96	108
4814.26	Cr I	3.09	-1.211	MFK	—	—	50	—	42	—
4836.85	Cr I	3.10	-1.137	MFK	43	—	—	—	63	—
4936.34	Cr I	3.11	-0.220	MFK	—	—	—	—	—	86
4964.93	Cr I	0.94	-2.526	MFK	—	107	—	—	—	—
5193.50	Cr I	3.42	-0.720	MFK	—	—	36	41	31	30
5200.18	Cr I	3.38	-0.650	MFK	—	—	63	59	62	—
5214.13	Cr I	3.37	-0.740	MFK	—	—	35	39	36	39
5238.96	Cr I	2.71	-1.305	MFK	35	62	46	—	42	52
5247.57	Cr I	0.96	-1.630	MFK	—	—	—	146	141	—
5272.00	Cr I	3.45	-0.421	MFK	—	77	47	49	47	—
5296.70	Cr I	0.98	-1.390	GS	142	—	144	157	—	—
5300.75	Cr I	0.98	-2.130	GS	—	134	107	116	114	123
5304.18	Cr I	3.46	-0.692	MFK	—	—	34	49	39	30
5318.77	Cr I	3.44	-0.688	MFK	—	—	—	43	38	—
5348.33	Cr I	1.00	-1.290	GS	136	—	150	—	—	—
5628.65	Cr I	3.42	-0.772	MFK	—	—	33	37	23	—
5702.32	Cr I	3.45	-0.666	MFK	52	—	70	63	60	—
5783.07	Cr I	3.32	-0.500	MFK	50	73	60	64	60	63
5783.87	Cr I	3.32	-0.290	GS	77	—	86	91	97	—
5784.97	Cr I	3.32	-0.379	MFK	—	80	—	63	66	—
5787.93	Cr I	3.32	-0.080	GS	66	98	78	84	82	85
6330.10	Cr I	0.94	-2.920	R03	68	121	83	83	87	89
4904.42	Ni I	3.54	-0.170	MFK	—	—	115	—	—	—
4913.98	Ni I	3.74	-0.620	MFK	77	—	82	93	83	100
4935.83	Ni I	3.94	-0.360	MFK	82	87	81	93	91	98
4953.21	Ni I	3.74	-0.660	MFK	86	—	87	96	94	95
4967.52	Ni I	3.80	-1.570	MFK	—	—	—	39	32	—
4995.66	Ni I	3.63	-1.580	MFK	—	51	38	—	45	—
5010.94	Ni I	3.63	-0.870	MFK	74	80	—	83	78	86
5084.11	Ni I	3.68	-0.180	E93	107	—	102	124	107	138
5094.42	Ni I	3.83	-1.080	MFK	49	59	56	63	55	—
5115.40	Ni I	3.83	-0.280	R03	103	—	97	—	111	125
5157.98	Ni I	3.61	-1.590	MFK	—	—	44	50	46	—
5197.17	Ni I	3.90	-1.190	MFK	—	—	59	70	61	62
5578.73	Ni I	1.68	-2.640	MFK	107	—	104	118	113	121
5589.37	Ni I	3.90	-1.140	MFK	—	56	46	53	48	61
5593.75	Ni I	3.90	-0.840	MFK	70	73	74	78	73	83
5643.09	Ni I	4.17	-1.250	MFK	—	38	26	38	30	—
5748.36	Ni I	1.68	-3.260	MFK	—	—	74	83	78	—
5760.84	Ni I	4.11	-0.800	MFK	64	—	73	58	71	80
5805.23	Ni I	4.17	-0.640	MFK	61	66	64	72	66	83
5996.74	Ni I	4.24	-1.060	MFK	38	—	46	53	48	57
6053.69	Ni I	4.24	-1.070	MFK	—	52	—	—	54	58
6086.29	Ni I	4.27	-0.510	MFK	59	76	72	83	73	—
6108.12	Ni I	1.68	-2.440	MFK	116	—	117	120	122	—
6111.08	Ni I	4.09	-0.870	MFK	55	67	61	64	61	72
6128.98	Ni I	1.68	-3.320	MFK	74	—	76	84	84	94
6130.14	Ni I	4.27	-0.960	MFK	40	47	40	50	47	49
6176.82	Ni I	4.09	-0.264	R03	88	97	85	100	93	114
6177.25	Ni I	1.83	-3.510	MFK	45	67	49	56	52	66
6186.72	Ni I	4.11	-0.960	MFK	51	60	52	64	54	58
6204.61	Ni I	4.09	-1.140	MFK	47	—	53	61	58	59
6223.99	Ni I	4.11	-0.980	MFK	—	—	60	61	48	—
6230.10	Ni I	4.11	-1.260	MFK	—	—	—	52	57	61
6322.17	Ni I	4.15	-1.170	MFK	32	—	37	47	34	—
6327.60	Ni I	1.68	-3.113	MFW	88	—	—	109	103	—
6378.26	Ni I	4.15	-0.900	MFK	56	—	—	71	72	—
6384.67	Ni I	4.15	-1.130	MFK	47	—	43	52	46	—
6482.80	Ni I	1.94	-2.630	MFW	81	—	100	108	101	—
6532.88	Ni I	1.94	-3.390	MFK	67	69	50	64	124	—

6586.33	Ni I	1.95	-2.810	MFW	85	—	90	98	96	—
6598.61	Ni I	4.24	-0.980	MFK	42	—	43	57	47	—
6635.14	Ni I	4.42	-0.830	MFK	50	—	—	—	55	—
6643.64	Ni I	1.68	-2.030	MFW	142	—	—	—	—	—
6767.77	Ni I	1.83	-2.170	MFW	125	—	—	—	—	—
6772.32	Ni I	3.66	-0.970	R03	70	84	80	—	98	—
6842.04	Ni I	3.66	-1.477	MFK	47	65	69	—	58	—
7788.93	Ni I	1.95	-1.990	E93	—	—	141	—	—	—
4883.68	Y II	1.08	0.070	SN96	—	—	145	—	—	—
5087.43	Y II	1.08	-0.170	SN96	123	142	115	124	119	—
5200.41	Y II	0.99	-0.570	SN96	—	—	109	112	116	—
5205.72	Y II	1.03	-0.340	SN96	—	—	134	—	—	—
5289.81	Y II	1.03	-1.850	VWR	49	74	55	46	56	64
5402.78	Y II	1.84	-0.440	R03	78	85	66	66	75	93
6127.46	Zr I	0.15	-1.060	H82	20	96	36	29	36	39
6134.57	Zr I	0.00	-1.280	B81	21	93	35	30	36	32
6140.46	Zr I	0.52	-1.410	S96	—	43	12	—	—	—
6143.18	Zr I	0.07	-1.100	B81	24	106	46	40	43	39
4934.83	La II	1.25	-0.920	VWR	35	—	28	—	34	37
5303.53	La II	0.32	-1.350	VWR	54	—	42	39	42	50
5880.63	La II	0.23	-1.830	R04	—	87	36	—	36	—
6320.42	La II	0.17	-1.520	VWR	41	124	47	38	65	47
6390.48	La II	0.32	-1.410	S96	54	115	55	42	53	53
6774.33	La II	0.12	-1.709	S96	52	119	44	39	47	50
4562.37	Ce II	0.48	0.330	S96	87	116	—	—	85	—
4628.16	Ce II	0.52	0.260	S96	—	—	—	—	95	—
5117.17	Ce II	1.40	0.010	VWR	28	—	26	—	—	38
5187.46	Ce II	1.21	0.300	VWR	51	86	—	—	47	57
5274.24	Ce II	1.28	0.389	VWR	58	80	53	49	57	72
5330.58	Ce II	0.87	0.280	VWR	—	—	—	36	—	—
5472.30	Ce II	1.25	-0.190	VWR	40	61	33	24	40	30
6051.80	Ce II	0.23	-1.600	S96	20	51	17	10	20	—
4811.34	Nd II	0.06	-1.015	VWR	71	—	67	—	69	87
4959.12	Nd II	0.06	-0.916	VWR	86	—	—	—	—	105
4989.95	Nd II	0.63	-0.624	VWR	57	—	—	—	—	—
5063.72	Nd II	0.98	-0.758	VWR	—	—	—	—	32	—
5092.80	Nd II	0.38	-0.510	E93	—	91	—	—	—	—
5130.59	Nd II	1.30	0.100	SN96	—	—	—	38	—	—
5212.36	Nd II	0.20	-0.700	E93	79	—	83	—	92	—
5234.19	Nd II	0.55	-0.460	S96	—	—	—	—	—	73
5311.46	Nd II	0.98	-0.560	SN96	—	—	49	—	—	—
5319.81	Nd II	0.55	-0.350	SN96	—	—	74	63	—	—
5416.38	Nd II	0.86	-0.980	VWR	—	50	—	—	—	—
5431.54	Nd II	1.12	-0.457	VWR	—	58	29	—	33	—
5442.26	Nd II	0.68	-0.900	SN96	46	—	—	—	54	65
5740.88	Nd II	1.16	-0.560	VWR	—	—	26	29	40	32
5842.39	Nd II	1.28	-0.601	VWR	—	40	—	—	—	—

**Table 4.** Other lines studied.

$\lambda(\text{\AA})$	Species	$\chi(\text{eV})$	$\log g f$	Ref	Equivalent widths (m\AA)						
					HD 100012	HD 101079	HD 130386	HD 139660	HD 198590	HD 212209	
6154.22	Na I	2.10	-1.510	R03	106	91	111	106	94	117	
6160.75	Na I	2.10	-1.210	R03	120	106	125	123	112	124	
4730.04	Mg I	4.34	-2.390	R03	121	—	114	—	113	—	
5711.10	Mg I	4.34	-1.750	R99	141	132	143	148	138	156	
6318.71	Mg I	5.11	-1.940	Ca07	76	69	84	76	78	—	
6319.24	Mg I	5.11	-2.160	Ca07	59	—	63	—	—	81	
6319.49	Mg I	5.11	-2.670	Ca07	46	37	41	40	41	49	
6765.45	Mg I	5.75	-1.940	MR94	35	40	—	—	32	49	
6965.41	Mg I	5.75	-1.720	MR94	91	65	77	82	73	83	
7387.70	Mg I	5.75	-0.870	MR94	98	97	102	107	—	—	
8712.69	Mg I	5.93	-1.260	WSM	110	—	96	—	—	89	
8717.83	Mg I	5.91	-0.970	WSM	124	116	114	112	125	106	
8736.04	Mg I	5.94	-0.340	WSM	—	159	161	156	—	165	
6696.03	Al I	3.14	-1.481	MR	91	79	90	90	79	104	
6698.67	Al I	3.14	-1.630	R03	—	—	80	70	—	90	
7835.32	Al I	4.04	-0.580	R03	90	85	92	82	84	101	
7836.13	Al I	4.02	-0.400	R03	94	94	101	99	94	113	
8772.88	Al I	4.02	-0.250	R03	121	—	110	135	127	132	
8773.91	Al I	4.02	-0.070	R03	—	140	152	—	—	162	
5793.08	Si I	4.93	-2.060	R03	75	73	80	81	82	—	
6125.03	Si I	5.61	-1.540	E93	58	56	70	66	62	71	
6131.58	Si I	5.62	-1.685	E93	46	50	54	55	59	47	
6145.02	Si I	5.61	-1.430	E93	61	60	58	63	63	58	
6155.14	Si I	5.62	-0.770	E93	110	100	105	108	109	110	
7760.64	Si I	6.20	-1.280	E93	39	31	—	51	45	36	
7800.00	Si I	6.18	-0.720	E93	93	80	78	—	95	86	
8728.01	Si I	6.18	-0.360	E93	107	111	93	104	118	99	
8742.45	Si I	5.87	-0.510	E93	102	114	106	129	127	—	
6161.30	Ca I	2.52	-1.270	E93	—	—	—	122	114	124	
6166.44	Ca I	2.52	-1.140	R03	117	107	115	113	109	122	
6169.04	Ca I	2.52	-0.800	R03	140	131	146	147	140	159	
6169.56	Ca I	2.53	-0.480	DS91	157	147	—	—	—	—	
6455.60	Ca I	2.51	-1.290	R03	109	100	118	117	106	126	
6471.66	Ca I	2.51	-0.690	S86	143	134	147	145	139	145	
4758.12	Ti I	2.25	0.425	MFK	89	—	—	—	—	—	
4759.28	Ti I	2.25	0.514	MFK	—	85	94	92	—	101	
4997.10	Ti I	0.00	-2.118	MFK	106	87	103	102	—	123	
5009.66	Ti I	0.02	-2.259	MFK	116	—	—	—	—	—	
5016.17	Ti I	0.85	-0.574	MFK	131	118	142	132	129	—	
5022.87	Ti I	0.83	-0.434	MFK	146	125	141	136	128	—	
5039.96	Ti I	0.02	-1.130	MFK	—	135	161	—	152	—	
5043.59	Ti I	0.84	-1.733	MFK	83	70	95	89	—	108	
5062.10	Ti I	2.16	-0.464	MFK	59	52	71	64	46	81	
5087.06	Ti I	1.43	-0.840	E93	—	80	—	—	79	—	
5113.45	Ti I	1.44	-0.880	E93	85	69	—	76	62	—	
5145.47	Ti I	1.46	-0.574	MFK	96	82	101	97	88	112	
5147.48	Ti I	0.00	-2.012	MFK	124	110	—	—	—	139	
5152.19	Ti I	0.02	-2.024	MFK	121	91	110	—	—	137	
5219.71	Ti I	0.02	-2.292	MFK	108	97	118	113	95	—	
5223.63	Ti I	2.09	-0.559	MFK	66	47	66	61	44	87	
5295.78	Ti I	1.05	-1.633	MFK	60	51	69	64	49	81	
5490.16	Ti I	1.46	-0.937	MFK	83	63	90	83	61	100	
5662.16	Ti I	2.32	-0.109	MFK	81	70	87	84	73	—	
5689.48	Ti I	2.30	-0.469	MFK	54	48	67	62	39	72	
5866.46	Ti I	1.07	-0.871	E93	129	116	—	—	—	—	
5922.12	Ti I	1.05	-1.465	MFK	89	71	86	98	84	106	
5978.55	Ti I	1.87	-0.496	MFK	83	69	85	84	68	100	
6091.18	Ti I	2.27	-0.370	R03	61	52	76	68	57	83	
6126.22	Ti I	1.05	-1.370	R03	90	80	100	93	77	111	

6258.11	Ti I	1.44	-0.355	MFK	119	105	123	113	111	136
6261.10	Ti I	1.43	-0.480	B86	136	113	—	—	115	—
6554.24	Ti I	1.44	-1.219	MFK	88	66	92	85	61	115
4789.34	Cr I	2.54	-0.365	MFK	—	—	—	116	—	—
4801.03	Cr I	3.12	-0.130	MFK	96	90	96	95	91	99
4814.26	Cr I	3.09	-1.211	MFK	—	51	—	—	—	—
4836.85	Cr I	3.10	-1.137	MFK	58	—	65	—	—	70
4936.34	Cr I	3.11	-0.220	MFK	88	—	—	—	—	—
4964.93	Cr I	0.94	-2.526	MFK	—	—	—	—	—	116
5193.50	Cr I	3.42	-0.720	MFK	54	35	51	47	34	63
5200.18	Cr I	3.38	-0.650	MFK	69	62	66	67	59	81
5214.13	Cr I	3.37	-0.740	MFK	42	34	45	45	36	61
5238.96	Cr I	2.71	-1.305	MFK	50	62	52	—	—	—
5243.36	Cr I	3.39	-0.567	MFK	—	67	—	77	—	—
5247.57	Cr I	0.96	-1.630	MFK	—	136	—	—	144	—
5272.00	Cr I	3.45	-0.421	MFK	—	46	54	—	45	71
5300.75	Cr I	0.98	-2.130	GS	125	112	126	123	113	141
5304.18	Cr I	3.46	-0.692	MFK	45	39	49	50	39	55
5312.86	Cr I	3.45	-0.562	MFK	—	—	—	—	38	67
5318.77	Cr I	3.44	-0.688	MFK	47	40	53	53	41	59
5340.45	Cr I	3.44	-0.730	MFK	—	62	—	—	—	71
5628.65	Cr I	3.42	-0.772	MFK	40	33	42	—	33	61
5702.32	Cr I	3.45	-0.666	MFK	52	63	67	67	56	—
5781.75	Cr I	3.32	-0.750	MFK	66	—	—	—	—	—
5783.07	Cr I	3.32	-0.500	MFK	69	59	68	71	63	74
5783.87	Cr I	3.32	-0.290	GS	—	—	—	—	97	104
5784.97	Cr I	3.32	-0.379	MFK	—	59	69	77	65	86
5787.93	Cr I	3.32	-0.080	GS	89	80	90	89	84	94
6330.10	Cr I	0.94	-2.920	R03	94	83	103	98	83	118
4904.42	Ni I	3.54	-0.170	MFK	130	109	—	—	—	—
4913.98	Ni I	3.74	-0.620	MFK	99	86	88	91	89	98
4935.83	Ni I	3.94	-0.360	MFK	87	88	86	92	93	88
4953.21	Ni I	3.74	-0.660	MFK	102	92	101	98	100	—
4967.52	Ni I	3.80	-1.570	MFK	39	35	41	44	41	50
4995.66	Ni I	3.63	-1.580	MFK	46	43	45	55	45	—
5003.75	Ni I	1.68	-3.130	MFK	83	—	—	—	—	93
5010.94	Ni I	3.63	-0.870	MFK	83	73	—	—	—	81
5084.11	Ni I	3.68	-0.180	E93	—	107	112	111	114	—
5094.42	Ni I	3.83	-1.080	MFK	58	55	61	58	59	—
5115.40	Ni I	3.83	-0.280	R03	—	—	—	109	—	—
5157.98	Ni I	3.61	-1.590	MFK	46	44	49	51	48	53
5197.17	Ni I	3.90	-1.190	MFK	71	62	—	73	66	—
5578.73	Ni I	1.68	-2.640	MFK	121	100	—	—	—	—
5587.87	Ni I	1.94	-2.370	MFK	107	—	—	—	—	110
5589.37	Ni I	3.90	-1.140	MFK	53	50	55	55	53	61
5593.75	Ni I	3.90	-0.840	MFK	76	68	74	76	77	83
5643.09	Ni I	4.17	-1.250	MFK	40	32	35	39	35	—
5748.36	Ni I	1.68	-3.260	MFK	86	76	86	83	77	99
5760.84	Ni I	4.11	-0.800	MFK	84	75	80	76	—	—
5805.23	Ni I	4.17	-0.640	MFK	74	63	68	73	72	75
5847.01	Ni I	1.68	-3.440	MFK	82	—	—	—	—	95
5996.74	Ni I	4.24	-1.060	MFK	57	43	55	57	53	—
6053.69	Ni I	4.24	-1.070	MFK	—	50	59	62	60	—
6086.29	Ni I	4.27	-0.510	MFK	79	69	77	77	75	74
6108.12	Ni I	1.68	-2.440	MFK	132	118	128	129	118	133
6111.08	Ni I	4.09	-0.870	MFK	74	62	67	66	69	69
6128.98	Ni I	1.68	-3.320	MFK	90	79	92	93	89	104
6130.14	Ni I	4.27	-0.960	MFK	58	46	49	54	58	52
6176.82	Ni I	4.09	-0.264	R03	100	91	93	95	99	103
6177.25	Ni I	1.83	-3.510	MFK	62	51	59	61	59	69
6186.72	Ni I	4.11	-0.960	MFK	66	55	59	63	57	75
6204.61	Ni I	4.09	-1.140	MFK	60	54	67	67	59	—
6223.99	Ni I	4.11	-0.980	MFK	63	56	61	70	64	80
6230.10	Ni I	4.11	-1.260	MFK	—	51	57	56	—	—

6322.17	Ni I	4.15	-1.170	MFK	47	38	47	47	44	—
6327.60	Ni I	1.68	-3.113	MFW	112	97	—	—	106	—
6378.26	Ni I	4.15	-0.900	MFK	—	62	—	78	75	—
6384.67	Ni I	4.15	-1.130	MFK	—	46	49	53	49	57
6482.80	Ni I	1.94	-2.630	MFW	111	92	117	117	100	—
6532.88	Ni I	1.94	-3.390	MFK	—	49	—	60	58	81
6586.33	Ni I	1.95	-2.810	MFW	103	95	103	105	101	123
6598.61	Ni I	4.24	-0.980	MFK	58	52	—	55	55	69
6643.64	Ni I	1.68	-2.030	MFW	—	149	—	163	—	—
6767.77	Ni I	1.83	-2.170	MFW	—	139	—	—	—	—
6772.32	Ni I	3.66	-0.970	R03	96	90	96	98	97	94
6842.04	Ni I	3.66	-1.477	MFK	67	62	—	—	69	—
4883.68	Y II	1.08	0.070	SN96	—	—	—	154	—	—
5087.43	Y II	1.08	-0.170	SN96	93	114	118	130	131	117
5200.41	Y II	0.99	-0.570	SN96	99	111	114	—	124	118
5289.81	Y II	1.03	-1.850	VWR	26	52	52	49	58	54
5402.78	Y II	1.84	-0.440	R03	50	68	68	—	79	68
6127.46	Zr I	0.15	-1.060	H82	28	37	63	52	37	68
6134.57	Zr I	0.00	-1.280	B81	27	36	58	50	35	65
6140.46	Zr I	0.52	-1.410	S96	—	—	20	19	13	25
6143.18	Zr I	0.07	-1.100	B81	33	44	64	59	44	78
4086.71	La II	0.00	-0.160	VWR	—	—	—	97	98	—
4934.83	La II	1.25	-0.920	VWR	—	—	—	23	—	—
5303.53	La II	0.32	-1.350	VWR	33	40	35	37	37	41
5880.63	La II	0.23	-1.830	R04	26	22	38	36	38	39
6320.43	La II	0.17	-1.520	VWR	38	42	44	47	38	46
6390.48	La II	0.32	-1.410	S96	36	47	54	52	39	—
6774.33	La II	0.12	-1.709	S96	30	38	34	—	32	40
4073.47	Ce II	0.48	0.320	SN96	—	—	—	79	82	—
4120.84	Ce II	0.32	-0.240	S96	65	—	—	—	72	—
4486.91	Ce II	0.30	-0.360	S96	—	—	70	—	—	—
4562.37	Ce II	0.48	0.330	S96	80	79	86	76	82	84
4628.16	Ce II	0.52	0.260	S96	77	—	81	76	90	—
5117.17	Ce II	1.40	0.010	VWR	—	—	—	—	24	—
5187.46	Ce II	1.21	0.300	VWR	—	41	—	—	40	40
5274.24	Ce II	1.28	0.389	VWR	46	48	48	—	47	44
5472.30	Ce II	1.25	-0.190	VWR	21	21	29	—	22	20
6051.80	Ce II	0.23	-1.600	S96	13	15	20	18	15	21
4811.34	Nd II	0.06	-1.015	VWR	60	58	65	57	58	—
4989.95	Nd II	0.63	-0.624	VWR	50	56	—	49	49	—
5063.72	Nd II	0.98	-0.758	VWR	16	19	17	37	19	—
5092.80	Nd II	0.38	-0.510	E93	—	—	49	—	—	59
5212.36	Nd II	0.20	-0.700	E93	—	—	—	—	78	—
5234.19	Nd II	0.55	-0.460	S96	58	—	—	60	58	—
5311.46	Nd II	0.98	-0.560	SN96	38	40	—	36	37	—
5319.81	Nd II	0.55	-0.350	SN96	80	76	56	66	72	61
5416.38	Nd II	0.86	-0.980	VWR	—	15	—	—	16	—
5431.54	Nd II	1.12	-0.457	VWR	—	27	—	—	23	—
5442.26	Nd II	0.68	-0.900	SN96	49	—	—	—	—	—
5740.88	Nd II	1.16	-0.560	VWR	20	21	—	28	20	33
5842.39	Nd II	1.28	-0.601	VWR	—	31	15	—	11	—

2

<sup>2</sup> References to Table 4:

References to Table 4:

B81: Biemont et al. (1981);

Ca07: Carretta et al. (2007);

DS91: Drake &amp; Smith (1991);

E93: Edvardsson et al. (1993);

GS: Gratton &amp; Sneden (1988);

H82: Hannaford et al. (1982);

PS: Preston &amp; Sneden (2001);

R03: Reddy et al. (2003);

R04: Reyniers et al. (2004);

MFK: Martin et al. (2002);

MFW: Martin et al. (1988);

MR94: McWilliam &amp; Rich (1994);

S86: Smith et al. (1986);

S96: Smith et al. (1996);

SN96: Sneden et al. (1996);

VWR: Van Winckel &amp; Reyniers (2000);

WSM: Wiese et al. (1969);